

Ultra Fast PDE Solving via Physics Guided Few-step Diffusion

Cindy Xiangrui Kong¹, Yueqi Wang¹, Haoyang Zheng¹, Weijian Luo² and Guang Lin¹

¹Purdue University, ²hi-Lab, Xiaohongshu Inc

Diffusion-based models have demonstrated impressive accuracy and generalization in solving partial differential equations (PDEs). However, they still face significant limitations, such as high sampling costs and insufficient physical consistency, stemming from their many-step iterative sampling mechanism and lack of explicit physics constraints. To address these issues, we propose *Phys-Instruct*, a novel physics-guided distillation framework which not only (1) compresses a pre-trained diffusion PDE solver into a few-step generator via matching generator and prior diffusion distributions to enable rapid sampling, but also (2) enhances the physics consistency by explicitly injecting PDE knowledge through a PDE distillation guidance. *Phys-Instruct* is built upon a solid theoretical foundation, leading to a practical physics-constrained training objective that admits tractable gradients. Across five PDE benchmarks, *Phys-Instruct* achieves *orders-of-magnitude faster inference* while reducing PDE error by *more than 8 \times* compared to state-of-the-art diffusion baselines. Moreover, the resulting unconditional student model functions as a compact prior, enabling efficient and physically consistent inference for various downstream conditional tasks. Our results indicate that *Phys-Instruct* is a novel, effective, and efficient framework for ultra-fast PDE solving powered by deep generative models.

1. Introduction

Diffusion models have recently shown strong empirical performance for modeling spatially structured scientific fields, and have been increasingly explored as flexible priors for *Partial Differential Equation (PDE)*-related data (Daras et al., 2024; Zheng et al., 2022, 2025b). In PDE solving problems, such priors are appealing not only for unconditional field generation, but also for conditional tasks such as forward prediction (Raissi et al., 2019), inverse problems (Cai et al., 2021; Zheng et al., 2024), and reconstruction from partial observations (Huang et al., 2024a). However, making diffusion models practical for PDE tasks requires addressing two coupled issues: sampling efficiency and physical consistency.

Sampling Efficiency. High-fidelity samples typically require hundreds to thousands of denoising steps, resulting in large numbers of function evaluations (NFE) and high sampling cost (Ho et al., 2020; Song et al., 2021). For example, DiffusionPDE (Huang et al., 2024a) addresses forward, inverse, and reconstruction PDE problems from sparse observations by running a long reverse diffusion trajectory on the order of thousands of steps; Yang and Sommer (2023) predicts nonlinear fluid fields with a denoising diffusion model that samples through hundreds of iterative Langevin updates. These approaches demonstrate the potential of diffusion-based PDE modeling, but the required number of function evaluations makes inference expensive and limits their practicality in real-world settings.

Physical Consistency. Standard diffusion training is primarily data-driven and does not explicitly enforce PDE governing equations; as a result, samples can be visually plausible yet exhibit non-negligible PDE error (Bastek et al., 2025). Moreover, under aggressive acceleration or data-free distillation, small distribution-matching errors can translate into noticeable physics violations, motivating explicit PDE-aware objectives (Zhang and Zou, 2025).

Existing physics-guided remedies tend to trade one challenge for the other: Some impose physics during inference via guidance or iterative correction, which can reduce PDE error but comes at the cost of higher sampling latency (Huang et al., 2024a). Others incorporate physics guidance during diffusion training by penalizing PDE error along multi-step denoising trajectories, but sampling typically remains iterative, and the additional constraints can introduce nontrivial trade-offs between sample quality and physical fidelity (Baldan et al., 2025; Bastek et al., 2025). In contrast, distillation and other aggressive acceleration schemes reduce sampling steps (Liu et al., 2023; Luo et al., 2023b; Salimans and Ho, 2022; Song et al., 2023), but physical consistency may degrade without explicit PDE equation constraint. This is particularly pronounced when the budget is limited, where fewer sampling steps imply more aggressive updates along the sampling trajectory, increasing approximation errors when physical constraints are enforced during inference. Together, these highlight a speed-physics trade-off in diffusion-based PDE generation.

In this paper, we address the mentioned issues by introducing **Phys-Instruct**, a physics-guided distillation framework that distills a multi-step diffusion teacher PDE solver into a few-step student solver, i.e., a few-step generator. Moreover, Phys-Instruct explicitly enforces physics consistency by adding physics equation constraint terms, e.g., differentiable PDE error, incorporating it into distillation as a novel constraint in (7). Importantly, this explicit constraint is applied only during training to shape the student distribution; at inference time, the student samples are obtained with a fixed few-step procedure and require no PDE-based guidance, correction, or post-hoc refinement. This few-step PDE solver obtained by Phys-Instruct can be used with flexibility.

We conduct evaluations of Phys-Instruct on a broad range of PDE benchmarks with varied formulations. Experiments show that adding physics guidance during distillation improves unconditional generation quality, yielding a favorable accuracy-latency trade-off relative to multi-step diffusion sampling. Crucially, the resulting distilled generator can be repurposed as a compact diffusion prior for conditional solvers. It facilitates efficient, non-iterative sampling across diverse PDE observation scenarios.

Our **main contributions** are three-fold: (i) we propose Phys-Instruct, a training-time physics-guided distillation framework that compresses a multi-step diffusion teacher into a one-/few-step generator for PDEs with no test-time physics guidance or control steps; (ii) we demonstrate that incorporating PDE error as a constraint improves distillation over the no physics guidance variant, while requiring no paired ground-truth training data supervision during distillation; (iii) We show the distilled unconditional generator serves as a reusable diffusion prior for downstream conditional PDE tasks (forward/inverse problem with full/partial observations), with favorable accuracy-latency trade-offs.

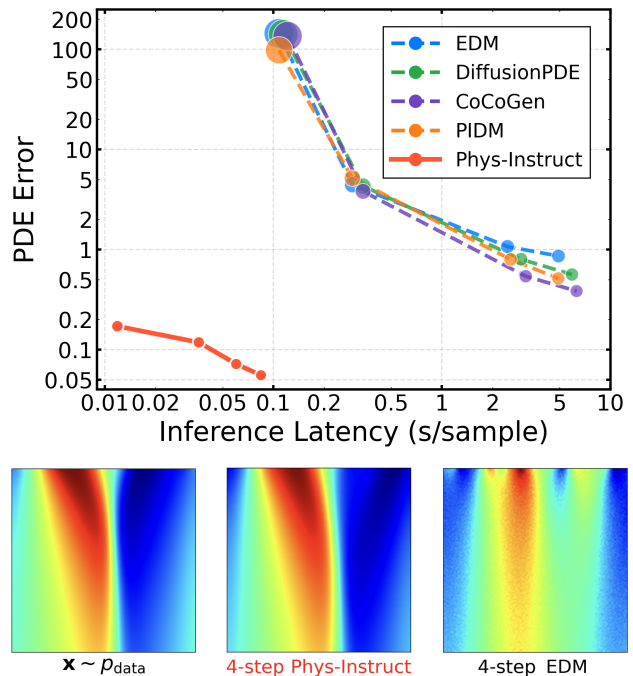


Figure 1 | Burgers’ unconditional generation. **Top:** PDE Error (lower is better, indicated by bubble size) vs. per-sample sampling latency. Baselines use 4/10/100/200 steps; Phys-Instruct uses 1–4 steps. **Bottom:** Unconditional Burgers’ samples (left to right): data from p_{data} , four-step Phys-Instruct, and four-step EDM teacher.

2. Related Work

2.1. Diffusion priors for PDE fields.

Recent work applies diffusion and score-based generative models to PDE fields in both unconditional and conditional settings. Unconditional models aim to learn the distribution of physically meaningful fields (Yuan et al., 2025), while conditional variants use diffusion priors to solve forward prediction, inverse problems, or reconstruction from partial observations by sampling fields consistent with given measurements (Baldassari et al., 2023; Shysheya et al., 2024). A central question in this field of literature is how to incorporate physics. Many approaches remain purely data-driven (Dasgupta et al., 2025; Wang et al., 2023), whereas physics-aware variants inject PDE structure through explicit regularization during training (Bastek et al., 2025; Shu et al., 2023) or through physics-guided sampling/correction along the generation trajectory (Huang et al., 2024a; Jacobsen et al., 2024; Yao et al., 2025). Our method is complementary: we incorporate physics only at *distillation time* to obtain efficient one-/few-step generators, without relying on test-time physics guidance or iterative correction.

2.2. Few-step diffusion and distillation.

Diffusion sampling is typically implemented by iteratively solving the reverse-time dynamics (e.g., via SDE/ODE solvers), and high-fidelity generation often requires many function evaluations (Karras et al., 2022; Song et al., 2021). A broad line of work reduces this cost through improved samplers and solver design (Dockhorn et al., 2022; Lu et al., 2022; Nichol and Dhariwal, 2021; Shih et al., 2023; Zhou et al., 2024b), as well as by distilling multi-step teachers into one-/few-step generators (Liu et al., 2023; Salimans and Ho, 2022). Consistency models enforce *trajectory consistency* across noise levels (Geng et al., 2025a,b; Kim et al., 2024; Lu and Song, 2025; Luo et al., 2023a; Song and Dhariwal, 2024; Song et al., 2023), while Diff-Instruct proposes a distribution-matching objective for one-step generation and has inspired many extensions (Fan et al., 2023; Huang et al., 2024b; Luo et al., 2023b, 2024a,b, 2025a,b; Wang et al., 2025; Xie et al., 2024; Xu et al., 2025; Yin et al., 2024a,b; Zheng et al., 2025a; Zhou et al., 2024a). Distillation is well-established in image or text generation, but adapting it to scientific generation is under explored, particularly in how to integrate physics constraints into the distillation process. Zhang and Zou (2025) apply distillation technique by explicitly enforcing PDE constraints on terminal samples, while Phys-Instruct enforces physics during distillation and therefore removes the need for inference-time physics guidance in both unconditional and conditional settings.

3. Background

3.1. Problem Setup of PDE Solvers

We consider PDE problems on a domain \mathcal{D} , where $\mathcal{D} = \Omega_x \subset \mathbb{R}^d$ for static systems and $\mathcal{D} = \Omega_x \times \Omega_t$ for dynamic systems. Let $\xi \in \mathcal{D}$ denote the coordinates. We collect all physical fields into $\mathbf{x}(\xi) \in \mathbb{R}^c$ and partition it as $\mathbf{x}(\xi) = [\mathbf{a}(\xi)^\top, \mathbf{u}(\xi)^\top]^\top$, where $\mathbf{a}(\xi) \in \mathbb{R}^{c_1}$, $\mathbf{u}(\xi) \in \mathbb{R}^{c_2}$, and $c = c_1 + c_2$. The pair (\mathbf{a}, \mathbf{u}) specifies a PDE instance and its associated solution: in static problems, \mathbf{a} represents coefficients and \mathbf{u} is the corresponding solution field; in dynamic problems, \mathbf{a} specifies the initial condition at $t = 0$ and $\mathbf{u} := \mathbf{u}(\cdot, T)$ denotes the solution state at a target time T . The governing laws, together with boundary/initial constraints, are written as

$$\mathcal{G}[\mathbf{x}](\xi) = 0, \quad \xi \in \Omega, \quad (1)$$

where \mathcal{G} is a differential operator. Our goal is to generate $\mathbf{x} = (\mathbf{a}, \mathbf{u})$ from the generator g_θ that satisfy (1).

3.2. Diffusion Models

Assume we observe data from an unknown distribution $\mathbf{x} \sim p_{\text{data}}(\mathbf{x})$. Diffusion models construct a forward noising process that transforms the initial distribution $p_0 = p_{\text{data}}$ into a simple noise distribution. Specifically, the forward process $\{\mathbf{x}_t\}_{t \in [0, T]}$ is described by the Itô SDE:

$$d\mathbf{x}_t = \mathbf{F}(\mathbf{x}_t, t) dt + G(t) d\mathbf{w}_t, \quad (2)$$

where \mathbf{F} and $G(t)$ are pre-defined drift and diffusion coefficients, and \mathbf{w}_t is a standard Wiener process. We write $p_t(\mathbf{x}_t)$ for the marginal density of \mathbf{x}_t and $p_{0t}(\mathbf{x}_t \mid \mathbf{x}_0)$ for the forward transition density induced by (2).

To reverse the noising dynamics, score-based diffusion models estimate the time-dependent score $\nabla_{\mathbf{x}_t} \log p_t(\mathbf{x}_t)$. Since it is intractable in high dimensions, we train a time-conditioned network $s_\phi(\mathbf{x}_t, t)$ to approximate it across noise levels. In practice, s_ϕ is implemented as a discrete noise-level network (Ho et al., 2020; Song and Ermon, 2019) or a continuous-time network (Karras et al., 2022; Song et al., 2021). Training is performed via minimizing a weighted denoising score matching objective (Song et al., 2021):

$$\mathcal{L}_{\text{DSM}}(\phi) = \int_0^T w(t) \mathbb{E}_{\mathbf{x}_0, \mathbf{x}_t \mid \mathbf{x}_0} \mathbf{g}_1 dt, \quad (3)$$

where $\mathbf{g}_1 := \|s_\phi(\mathbf{x}_t, t) - \nabla_{\mathbf{x}_t} \log p_{0t}(\mathbf{x}_t \mid \mathbf{x}_0)\|_2^2$, $\mathbf{x}_0 \sim p_0$, and $\mathbf{x}_t \mid \mathbf{x}_0 \sim p_{0t}(\mathbf{x}_t \mid \mathbf{x}_0)$, the weighting function $w(t)$ balances the contributions from different noise levels.

3.3. Integral Kullback-Leibler Divergence

Reverse (2) via iterative sampling typically requires a large number of sampling steps, leading to high inference latency, which can limit the practicality of diffusion models for PDE solving. This bottleneck can be alleviated by casting accelerated generation as a distillation problem: a multi-step teacher provides high-quality generative behavior, while a student is trained to produce comparable outputs in substantially fewer function evaluations. To encourage the student to learn the teacher’s evolution over time rather than only matching the final output, we adopt a distributional distillation framework that aligns their time-indexed marginals along the diffusion process.

Let $\{p_t(\mathbf{x}_t)\}_{t \in [0, T]}$ denote the teacher marginals induced by the forward diffusion (2), and let the teacher score be given by a frozen network $s_\nu(\mathbf{x}_t, t) \approx \nabla_{\mathbf{x}_t} \log p_t(\mathbf{x}_t)$. The student model induces a distribution $q_{\theta,0}$ over clean samples \mathbf{x}_0 (e.g., through a few-step generator), and we define its time- t marginals $\{q_{\theta,t}(\mathbf{x}_t)\}_{t \in [0, T]}$ by applying the same forward diffusion (2) to $\mathbf{x}_0 \sim q_{\theta,0}$, i.e., $\mathbf{x}_t \mid \mathbf{x}_0 \sim p_{0t}(\mathbf{x}_t \mid \mathbf{x}_0)$. Integral Kullback-Leibler (IKL) divergence generalizes the standard KL divergence by integrating the discrepancy between teacher and student marginals across all diffusion times, which was initially used in Luo et al. (2023b):

$$\begin{aligned} \mathcal{D}_{\text{IKL}}^{[0,T]}(q_\theta \| p) &:= \int_0^T w(t) \mathcal{D}_{\text{KL}}(q_{\theta,t} \| p_t) dt \\ &= \int_0^T w(t) \mathbb{E}_{\mathbf{x}_t \sim q_{\theta,t}} \left[\log \frac{q_{\theta,t}(\mathbf{x}_t)}{p_t(\mathbf{x}_t)} \right] dt, \end{aligned} \quad (4)$$

where $w(t) > 0$ weights the relative importance of different noise levels. Minimizing $\mathcal{D}_{\text{IKL}}^{[0,T]}$ promotes trajectory-level consistency between the student and teacher models is essential for high-quality sampling with limited budgets.

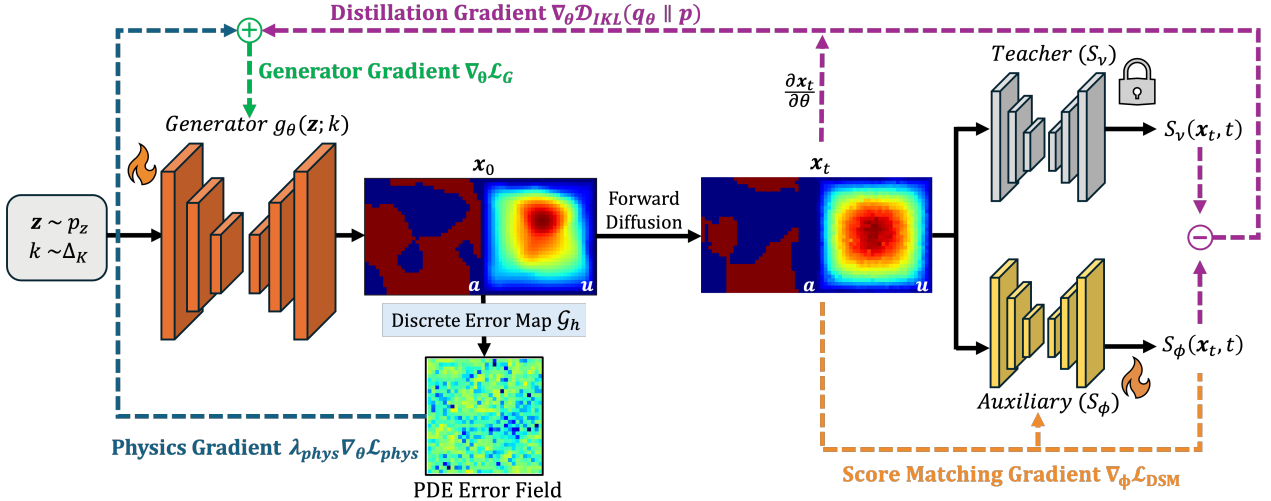


Figure 2 | **Overview of Phys-Instruct.** We sample latent variable $\mathbf{z} \sim p_z$, step budget $k \sim \Delta_K$, and generate PDE state $\mathbf{x}_0 = g_\theta(\mathbf{z}; k)$ with the generator g_θ . Then \mathbf{x}_0 is diffused to noisy state \mathbf{x}_t , which is evaluated by a frozen teacher diffusion model s_v and an auxiliary diffusion model s_ϕ . The auxiliary network is trained online via denoising score matching ($\nabla_\phi \mathcal{L}_{\text{DSM}}$). The generator g_θ is updated by the distillation gradient $\nabla_\theta \mathcal{D}_{\text{IKL}}(q_\theta \parallel p)$ plus a physics gradient $\nabla_\theta \mathcal{L}_{\text{phys}}$ weighted by a coefficient λ_{phys} .

4. Phys-Instruct

While the IKL objective in (4) provides a principled way to distill a multi-step diffusion teacher into a few-step student, matching the teacher distribution alone does not ensure that the student outputs satisfy the target PDE constraints. Existing physics-guided remedies often enforce feasibility at inference time through guidance or iterative correction, which increases the number of function evaluations and erodes the latency gains of few-step generation.

We therefore propose **Phys-Instruct**, a diffusion distillation framework that *instructs* a few-step student with physics guidance during training. Concretely, we distill a pretrained multi-step diffusion teacher into a *few-step* generator while simultaneously enforcing the PDE constraint (1) through a differentiable PDE error computed on generated samples. In this way, physics enters as explicit training-time supervision for the student, rather than as test-time guidance. As a result, Phys-Instruct produces PDE-consistent samples with a few-step sampler and requires no paired ground-truth solutions during distillation. Figure 2 provides a schematic overview of the proposed framework.

4.1. Phys-Instruct Generator

Luo et al. (2023b) distills a pretrained diffusion teacher into an *implicit one-step* sampler, mapping a Gaussian latent \mathbf{z} to a sample in a single network evaluation. While maximally fast, a single step can be overly restrictive for approximating the teacher’s multi-step sampling trajectory. Phys-Instruct generalizes this idea by enabling the student sampler to unroll a *small* number of sampling steps, yielding a distilled diffusion model which can take on step budget $k \in \{1, \dots, K\}$. This provides a simple knob to trade sampling quality for compute while preserving teacher-aligned sampling semantics. Specifically, we parameterize the student generator as a diffusion model g_θ and denote its output with k unrolled steps by $\mathbf{x}_0 = g_\theta(\mathbf{z}; k)$, where the latent variable $\mathbf{z} \sim p_z$.

Unified k -Step Formulation.

For a given step budget k and fixed noise level σ_{init} , we select $k+1$ noise levels from a fixed sampling schedule,

$$\sigma_k > \sigma_{k-1} > \dots > \sigma_0, \quad \sigma_k = \sigma_{\text{init}},$$

and draw the initial state $\mathbf{x}_k := \mathbf{z}$, with $\mathbf{z} \sim \mathcal{N}(\mathbf{0}, \sigma_{\text{init}}^2 \mathbf{I})$. We then iteratively apply a student-aligned step operator for k steps ,

$$\mathbf{x}_{i-1} = \text{Step}(\mathbf{x}_i; \sigma_i, \sigma_{i-1}, g_\theta), \quad i = k, k-1, \dots, 1,$$

where $\text{Step}(\cdot)$ belongs to the sampler family that the student diffusion model structure supports (e.g., the Euler or Heun sampler), and is parameterized by the student model g_θ . Notably, Phys-Instruct generates samples in k steps *without* any additional PDE-guided correction at inference time; physics guidance is injected only during distillation. We detail how this is achieved in the remainder of this section.

4.2. PDE Error and Physics Loss.

In practice, all physical fields are defined on a fixed discretized grid $\mathcal{D}_h = \{\xi_i\}_{i=1}^N \subset \Omega$. We approximate the continuous constraint \mathcal{G} in (1) on this grid with a differentiable *discrete PDE error map* \mathcal{G}_h , implemented using finite-difference stencils or convolutional filters. The resulting *PDE error (residual) field* is

$$r(\mathbf{x})_i := \mathcal{G}_h[\mathbf{x}](\xi_i), \quad i = 1, \dots, N, \quad (5)$$

and we summarize it into a scalar physics error via the mean squared PDE error

$$\mathcal{R}(\mathbf{x}) := \frac{1}{N} \sum_{i=1}^N \|r(\mathbf{x})_i\|_2^2. \quad (6)$$

When boundary conditions are prescribed, we impose them explicitly and compute the error only over interior (unconstrained) nodes, which reduces spurious errors introduced by boundary discretization.

4.3. Phys-Instruct Objective

Starting from IKL minimization in (4), we incorporate the physics guidance via (6). Conceptually, this corresponds to a *constrained* distillation problem that matches the teacher distribution while enforcing physical feasibility ¹:

$$\min_{\theta} \mathcal{D}_{\text{IKL}}(q_\theta \| p) \quad \text{s.t.} \quad \mathbb{E}_{\mathbf{x}_0 \sim q_\theta} [\mathcal{R}(\mathbf{x}_0)] \leq \varepsilon, \quad (7)$$

where $\mathcal{R}(\mathbf{x}_0) \geq 0$ denotes the PDE error evaluated on a generated sample \mathbf{x}_0 by the student, $\varepsilon > 0$ is some threshold. In our PDE setting, each \mathbf{x}_0 encodes the solution field together with the coefficient/forcing fields, and $\mathcal{R}(\mathbf{x}_0)$ is computed with (6).

Building on the unified k -step formulation in Sec. 4.1, we train a *single* student diffusion model that supports flexible sampling budgets $k \in \{1, \dots, K\}$ by randomly unrolling k steps during training. Concretely, we draw

$$k \sim \Delta_K \quad \text{over } \{1, \dots, K\},$$

¹We rewrite $\mathcal{D}_{\text{IKL}}^{[0,T]}(\cdot \| \cdot)$ as $\mathcal{D}_{\text{IKL}}(\cdot \| \cdot)$ unless stated otherwise.

where Δ_K is a categorical distribution over step budgets, and generate a student sample via the k -step generator $\mathbf{x}_0 = g_\theta(\mathbf{z}; k)$ with $\mathbf{z} \sim p_z$.

We define the physics guidance $\mathcal{L}_{\text{phys}}$ on student samples:

$$\mathcal{L}_{\text{phys}}(\theta) := \mathbb{E}_{\mathbf{z} \sim p_z, k \sim \Delta_K, \mathbf{x}_0 = g_\theta(\mathbf{z}; k)} [\mathcal{R}(\mathbf{x}_0)], \quad (8)$$

This term is applied *only* when updating the student generator: the teacher score network and the auxiliary score model are not directly regularized by $\mathcal{L}_{\text{phys}}$, preserving the original IKL distillation dynamics.

A central challenge is to relate the implemented guided generator update to an explicit distribution-matching objective. We propose a penalized IKL objective, where distillation is regularized by (8) to ensure the student matches the teacher subject to PDE satisfaction.

The next theorem introduces the penalized IKL objective obtained by augmenting IKL with the physics guidance term (8), and provides a score-function identity that decomposes its gradient into two parts: an IKL distribution-matching term in the spirit of Diff-Instruct and a PDE guidance term.

Theorem 4.1 (Score-Function Identity). *Consider the physics-constrained IKL matching problem (7). As a practical surrogate, we apply a Lagrangian relaxation of (7) and define the generator objective, treating $\lambda_{\text{phys}} > 0$ as a trade-off hyperparameter:*

$$\mathcal{L}_G(\theta) := \mathcal{D}_{\text{IKL}}(q_\theta \| p) + \lambda_{\text{phys}} \mathcal{L}_{\text{phys}}(\theta), \quad (9)$$

where $\mathcal{L}_{\text{phys}}(\theta)$ is given by (8). Under mild regularity conditions stated in Appendix B, the gradient of the implemented generator objective $\mathcal{L}_G(\theta)$ admits the identity

$$\begin{aligned} \nabla_\theta \mathcal{L}_G(\theta) &= \int_0^T w(t) \mathbb{E}_{\substack{\mathbf{z} \sim p_z, k \sim \Delta_K, \mathbf{x}_0 = g_\theta(\mathbf{z}; k), \\ \mathbf{x}_t \sim p_{0t}(\cdot | \mathbf{x}_0)}} \mathbf{g}_2 dt + \lambda_{\text{phys}} \mathbf{g}_3 \\ \text{where } \mathbf{g}_2 &:= \text{SG}\{s_\phi(\mathbf{x}_t, t) - s_\nu(\mathbf{x}_t, t)\}^\top \nabla_\theta \mathbf{x}_t, \\ \mathbf{g}_3 &:= \mathbb{E}_{\substack{\mathbf{z} \sim p_z, k \sim \Delta_K}} \left[(\nabla_{\mathbf{x}_0} \mathcal{R}(\mathbf{x}_0))^\top \nabla_\theta g_\theta(\mathbf{z}; k) \right]_{\mathbf{x}_0 = g_\theta(\mathbf{z}; k)}, \end{aligned} \quad (10)$$

SG(\cdot) denotes the stop-gradient operator, and $s_\phi(\mathbf{x}_t, t)$ is an auxiliary diffusion score model trained to approximate the marginal score $\nabla_{\mathbf{x}_t} \log q_{\theta, t}(\mathbf{x}_t)$ of the student-induced distribution at time t . Consequently, the gradient update implemented by (10) yields a stochastic estimator of the gradient of the penalized IKL objective with PDE guidance.

Proof. We employ Lagrange multipliers to reformulate the constrained optimization into an unconstrained objective comprising a distillation term and a physics-guidance penalty. For the distillation term, we apply the chain rule to the reparameterized diffusion process, decomposing the gradient into a score-matching component and a density sensitivity term. The latter vanishes under expectation due to the conservation of probability mass, which simplifies the update to a weighted integral of the teacher-student score difference. The physics guidance gradient is then derived straightforwardly via standard backpropagation of the penalty term. This completes the proof. We defer the detailed proof to Appendix B for interested readers. \square

It is worth noting that we evaluate the PDE error on each generated sample \mathbf{x}_0 , rather than on a mean prediction such as $\mathbb{E}[\mathbf{x}_0 | \mathbf{z}]$. This distinction is critical for nonlinear PDEs: optimizing the mean incurs a Jensen gap that conflicts with distribution matching (Zhang and Zou, 2025). By penalizing directly, we avoid this bias and ensure that individual samples (rather than just their aggregate expectation) adhere to physical laws.

Algorithm 1 Phys-Instruct.

```

1: Input: pre-trained model  $s_\nu$ ; generator  $g_\theta$ ; prior  $p_z$ ; auxiliary  $s_\phi$ ; regularization weight  $\lambda_{\text{phys}}$ ; max step  $K$ .
2: while not converge do
3:   // Score-learning phase for auxiliary diffusion model
4:   Sample  $\mathbf{z} \sim p_z$ ,  $k \sim \Delta_K$ , set  $\mathbf{x}_0 = g_\theta(\mathbf{z}; k)$  and diffuse to  $\mathbf{x}_t$  via the forward SDE (2).
5:   Update  $\phi$  using SGD with loss function (3).
6:   // Instruction + physics phase for generator
7:   Sample  $\mathbf{z} \sim p_z$ ,  $k \sim \Delta_K$ , set  $\mathbf{x}_0 = g_\theta(\mathbf{z}; k)$  and diffuse to  $\mathbf{x}_t$  via the forward SDE (2).
8:   Update  $\theta$  using SGD with loss function (9), whose tractable gradient is (10).
9: end while
10: Output:  $\theta, \phi$ .

```

Remark 4.2 (Amortized physics correction). The second term in (10) provides an explicit physics correction direction for the student generator. Indeed, for a fixed (\mathbf{z}, k) , the chain rule gives

$$\nabla_\theta \mathcal{R}(g_\theta(\mathbf{z}; k)) = \left(\nabla_{\mathbf{x}_0} \mathcal{R}(\mathbf{x}_0) \right)^\top \nabla_\theta g_\theta(\mathbf{z}; k) \Big|_{\mathbf{x}_0 = g_\theta(\mathbf{z}; k)}.$$

Thus, the physics-guided component in (10) pushes the generator outputs along $-\nabla_{\mathbf{x}_0} \mathcal{R}(\mathbf{x}_0)$, i.e., toward lower-residual samples. This can be viewed as amortizing a physics feasibility-improving correction into the student during training, thereby reducing the reliance on additional test-time guidance when operating at small step budgets.

4.4. Training Procedure

The Phys-Instruct distillation procedure assumes a pretrained diffusion model s_ν is given. The teacher diffusion models are trained with PDE data to reverse (2) that progressively adds noise to a sample from a real data distribution p_0 , where $R(\mathbf{x}_0^*) = 0$ if $\mathbf{x}_0^* \sim p_0$. The teacher diffusion model s_ν is freezed for the whole training procedure.

Phys-Instruct trains the student generator g_θ through two alternative phases between updating the auxiliary diffusion model s_ϕ , and updating the student generator g_θ , with both g_θ and s_ϕ initialized with the teacher's parameters. The former phase follows the standard diffusion model learning procedure, i.e., minimizing loss function (3), with a slight change that \mathbf{x}_0 is not from the training dataset but generated from g_θ . The resulting auxiliary model $s_\phi(\mathbf{x}_t, t)$ provides an estimation of $\log q_{\theta, t}(\mathbf{x}_t)$. The latter phase updates the generator's parameter θ using $\mathcal{L}_G(\theta)$, whose tractable gradient $\nabla_\theta \mathcal{L}_G(\theta)$ is derived as (10). When the training converges, $s_\phi \approx s_\nu$, and the gradient of (3) is approximately zero. The whole procedure is summarized in Algorithm 1.

5. Experiments

PDE Benchmarks.

We conduct experiments on 5 different PDE benchmarks, including Darcy flow, the Poisson equation, the non-bounded Navier-Stokes equation, the Burgers' equation, and the inhomogeneous Helmholtz equation. The dataset generation mainly follow released scripts in (Huang et al., 2024a) and (Li et al., 2021). Different benchmarks are of different resolutions as indicated in Table 1. More details about the PDE benchmarks are deferred to Appendix A.

Table 1 | Unconditional generation results on PDE benchmarks. We report PDE Error \downarrow and the number of sampling steps per sample (Step). NS_{unb.} denotes the nonbounded Navier–Stokes benchmark, and the lowest PDE Error for each benchmark is **bolded**.

Method	Step	PDE Error (\downarrow)				
		Darcy Flow	Poisson	NS _{unb.}	Burgers	Helmholtz
Resolution		32×32×2	32×32×2	64×64×2	128×128×1	128×128×2
Phys-Instruct	1	3.15×10^{-1}	2.16×10^{-2}	3.15×10^{-2}	1.71×10^{-1}	3.75×10^{-1}
	2	2.18×10^{-1}	5.18×10^{-3}	1.46×10^{-2}	1.18×10^{-1}	3.00×10^{-1}
	3	1.35×10^{-1}	4.79×10^{-3}	3.65×10^{-3}	7.17×10^{-2}	2.10×10^{-1}
	4	8.49×10^{-2}	3.99×10^{-3}	3.21×10^{-3}	5.54×10^{-2}	1.46×10^{-1}
EDM (Karras et al., 2022)	4	196.03	16.72	3.33×10^{-1}	144.23	79.77
DiffusionPDE (Huang et al., 2024a)	4	191.50	16.68	3.30×10^{-1}	141.37	78.97
CoCoGen (Jacobsen et al., 2024)	4	190.87	16.60	3.24×10^{-1}	135.65	77.34
PIDM (Bastek et al., 2025)	4	101.04	22.64	3.44×10^{-1}	97.76	77.86
EDM (Karras et al., 2022)	200	5.59×10^{-1}	3.14×10^{-2}	3.60×10^{-2}	8.60×10^{-1}	3.54×10^{-1}
DiffusionPDE (Huang et al., 2024a)	200	4.38×10^{-1}	2.64×10^{-2}	3.23×10^{-2}	5.62×10^{-1}	3.38×10^{-1}
CoCoGen (Jacobsen et al., 2024)	200	3.31×10^{-1}	1.40×10^{-2}	2.92×10^{-2}	3.84×10^{-1}	3.04×10^{-1}
PIDM (Bastek et al., 2025)	200	5.26×10^{-1}	2.36×10^{-2}	3.54×10^{-2}	5.14×10^{-1}	3.15×10^{-1}

Training.

For all benchmarks, Phys-Instruct utilizes the EDM teacher model (Karras et al., 2022) and jointly generates both the coefficient field \mathbf{a} and the solution field \mathbf{u} , except for the Burgers’ equation benchmark, where we store only the space–time field \mathbf{u} . Teacher models are trained with 50,000 data points. The teacher models for Darcy flow, Poisson, and non-bounded Navier-Stokes are trained with 4 V100 GPUs for 6 hours. The teacher models for Burgers’ and Helmholtz come from (Huang et al., 2024a). The step operator follows the deterministic second-order Heun sampler in (Karras et al., 2022). The distillation is conducted with $K = 4$ with 2 A100 GPUs for around 4 hours.

Baselines and Protocols.

We evaluate four diffusion-based baselines using the deterministic second-order Heun sampler following (Karras et al., 2022). To assess both generation quality and computational efficiency, we report results at 200 steps representing the baselines’ full potential, and at 4 steps matching the budget of our proposed method. Our comparison includes the plain EDM teacher model (Karras et al., 2022) as a purely data-driven reference without physical constraints. We then consider two methods that enforce physics during sampling: DiffusionPDE (Huang et al., 2024a) augments EDM by injecting physics guidance specifically during the final 20% of the sampling trajectory following diffusion posterior sampling (DPS) (Chung et al., 2023), with this guidance extending to the last 50% when step=4. Similarly, CoCoGen (Jacobsen et al., 2024) starts from the DiffusionPDE output and performs an additional ten-step physics-guided refinement, or two extra steps specifically for the four-step setting. Finally, we compare against PIDM (Bastek et al., 2025), which distinguishes itself by incorporating physics guidance directly into the training objective rather than during sampling.

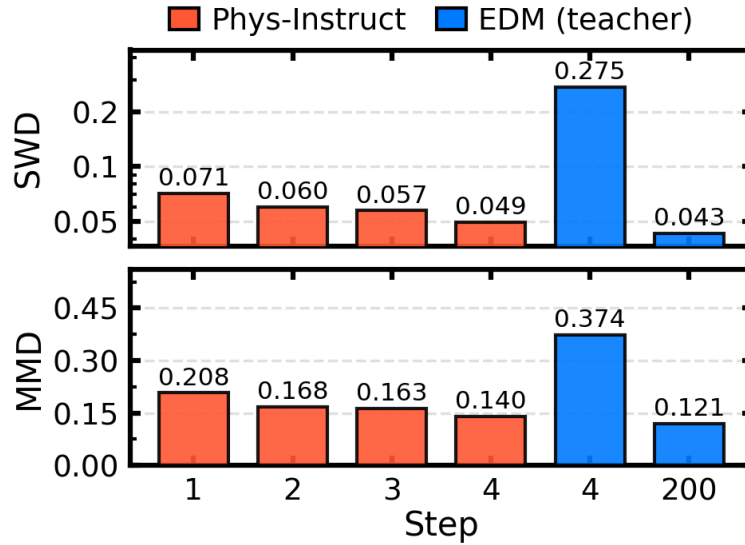


Figure 3 | Distributional discrepancy on the Burgers' equation benchmark measured by sliced Wasserstein distance (SWD, top) and Maximum Mean Discrepancy (MMD, bottom; reported as $\sqrt{MMD^2}$), where lower is better.

5.1. Main Results

As our primary physics consistency metric, we report $PDE\ Error \downarrow$, the root-mean-square of the PDE error computed per sample as $\sqrt{\mathcal{R}(\mathbf{x}_0)}$ and then averaged over samples; the results are summarized in Table 1. The efficiency trade-off is visualized in Figure 1, and the distributional discrepancy, measured by SWD and MMD, is reported in Figure 3.

It is shown in Table 1 that Phys-Instruct is particularly effective in the low-step regime. Increasing the sampling steps from 1 to 4 yields consistent improvements in PDE error across all benchmarks. Figure 6 further provides qualitative generation results of Darcy flow with 1-4 step Phys-Instruct. Notably, the one-step Phys-Instruct already outperforms the best Darcy flow and Burgers' baseline even when the baseline uses 200 sampling steps, and the four-step Phys-Instruct attains the lowest PDE error overall. In contrast, at the same low sampling budget (Step=4), diffusion baselines often produce samples with substantially larger PDE error. With such aggressive step sizes, the correction evaluation in second-order samplers can become sensitive to model and discretization errors, which may degrade the final sample quality, as illustrated in Figure 1. Phys-Instruct alleviates this issue because the student is distilled with the Heun sampler at fixed noise levels, i.e., it matches the teacher along a specific discrete trajectory. This effectively learns a discrete transport map tailored to the few-step schedule, rather than relying on large-step integration of the teacher's continuous-time dynamics.

The efficiency advantage is further illustrated in Figure 1. Latency measures end-to-end sampling time and includes any physics guidance or refinement applied during sampling. Diffusion baselines exhibit a clear compute-quality trade-off: achieving lower PDE error typically requires substantially more sampling steps, whereas very small step budgets often degrade physics consistency. In contrast, Phys-Instruct attains low PDE error at significantly lower latency. Increasing the student budget from Step=1 to Step=4 yields consistent improvements on Burgers', reducing PDE error from 1.71×10^{-1} to 5.54×10^{-2} , while remaining in the low-latency regime.

Beyond physics consistency, we measure distributional discrepancy to held-out data on Burgers

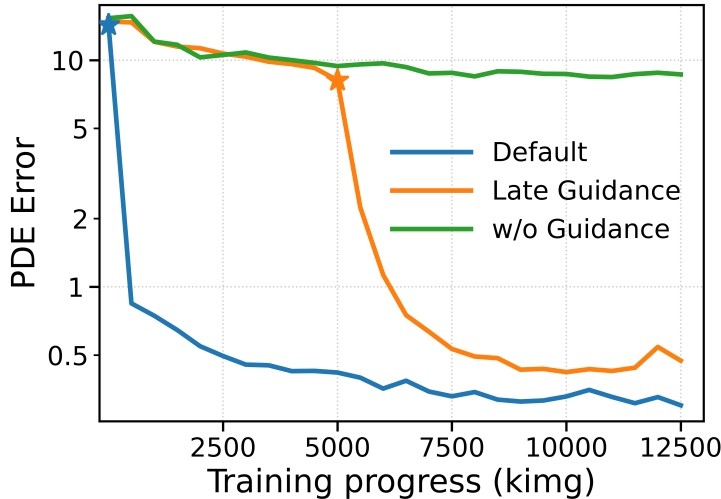


Figure 4 | Darcy-flow PDE error with one dtep Phys-Instruct during distillation under different physics-guidance schedules; stars indicate when guidance starts.

using SWD and MMD, reported in Figure 3. Few-step Phys-Instruct substantially improves both metrics compared to low-budget teacher sampling. At Step= 4, SWD and MMD improve by 82% and 63%, respectively. Meanwhile, the four-step Phys-Instruct achieves SWD and MMD that are comparable to those of the high-budget EDM teacher, albeit slightly worse. These results indicate effective distillation and suggest that incorporating physics guidance during training does not induce mode collapse. The remaining gap is expected, since Phys-Instruct is distilled from the teacher under a constrained step budget rather than directly optimizing SWD/MMD to match the data distribution.

5.2. Ablation Studies

We ablate the role of physics guidance in Phys-Instruct to understand how it improves physical consistency. Table 2 reports results on Darcy flow with fixed $\sigma_{\text{init}} = 1.5$ under one-step sampling, measured by the PDE Error. Removing PDE guidance (w/o Guidance) leads to degradation in physics consistency, with a PDE Error of 8.75 on Darcy flow. In contrast, adding the physics guidance with the default weight ($\lambda_{\text{phys}} = 5 \times 10^{-3}$) decreases PDE Error by approximately 27 times. Figure 4 further illustrates the training dynamics. The trajectory without physics guidance plateaus at a high PDE Error, whereas applying physics guidance from the start drives a faster and more sustained decrease in PDE Error. When guidance is activated only after the PDE error plateaus, the error decreases after the intervention, but does not fully match the best performance. Overall, these results indicate that PDE guidance provides an effective optimization signal and that introducing it throughout distillation yields the best result.

Additionally, Table 2 indicates that the method is reasonably robust to the choice of λ_{phys} within a practical range. Overly weak physics weighting noticeably degrades physical consistency, whereas a larger weight performs comparably to the default. Additional sensitivity analyses for λ_{phys} and σ_{init} are provided in Appendix D.

5.3. Downstream tasks

We further show that the distilled few-step students provide strong *unconditional priors* for downstream PDE tasks, including forward and inverse problems. Specifically, we freeze the unconditional Phys-

Table 2 | Ablation of Physics guidance in **one-step** Phys-Instruct training on Darcy flow. **Default** denotes our full training configuration. We report the PDE Error (↓). k_{img} indicates the starting point of adding physics guidance.

Setting	Guidance	k_{img}	λ_{phys}	PDE Error↓
Default	✓	0	5e-3	3.15×10^{-1}
w/o Guidance	✗	–	0	8.75
Late Guidance	✓	5k	5e-3	4.07×10^{-1}
Weak Guidance	✓	0	1e-3	3.59×10^{-1}
Strong Guidance	✓	0	1e-2	3.18×10^{-1}

Table 3 | Helmholtz forward problem. We report prediction error and PDE Error (↓). Step denotes the number of sampling steps per sample.

Method	Step	Helmholtz	
		Rel. Error	PDE Error
PhysInstruct	1	1.86%	4.18×10^{-1}
DiffusionPDE	2000	9.69%	1.48
CoCoGen	2000	9.70%	1.07
PIDM	2000	13.76%	1.36

Instruct student as a backbone prior and attach a ControlNet-style conditional branch (Zhang et al., 2023) to incorporate observations. Due to space constraints, details of the conditional pipeline implementation and baselines are deferred to Appendix E. We showcase the forward problem on Helmholtz and the inverse problem on Darcy flow and Poisson in this section. Extra downstream task experiments can be found in Appendix F.

Table 3 shows that, despite using only one sampling step, Phys-Instruct achieves substantially better Helmholtz forward accuracy and physics consistency than diffusion baselines that require 2000 steps. In particular, Phys-Instruct reduces the relative error by about 5–7 times and lowers the PDE Error by roughly 2.5–3.5 times compared to the 2000-step methods. In Figure 7, we visualize the results for solving the forward problem of the Helmholtz equation. A similar trend holds for inverse problems in Table 4. On Darcy flow, Phys-Instruct improves the absolute error by around 15–20 times and reduces the PDE Error by about 7–8 times relative to the 2000-step baselines. On Poisson, Phys-Instruct achieves a 1.5–2 times reduction in relative error and a 5–6 times reduction in PDE Error. Overall, Phys-Instruct delivers multi-fold gains in both accuracy and physics consistency while operating at orders-of-magnitude lower sampling cost.

6. Conclusion and Future Work

We propose Phys-Instruct, a physics-guided distillation framework that compresses a diffusion teacher into a few-step generator for PDE solution generation. Phys-Instruct augments IKL-based distillation objective with physics constraints, yielding students that produce physically consistent samples with dramatically fewer function evaluations. Empirically, the few-step Phys-Instruct achieves substantially lower PDE Error than diffusion baselines that require hundreds of sampling steps, and the distilled one-step model serves as a strong unconditional backbone for downstream conditional tasks. Since Phys-Instruct does not rely on test-time physics correction, it enables fast inference while retaining high physical fidelity.

Table 4 | Inverse problems on Darcy flow and Poisson equation. We report prediction error and PDE Error (↓). Prediction error is absolute error for Darcy flow and relative error for Poisson. Step denotes the number of sampling steps per sample.

Inverse	Darcy Flow			Poisson		
	Method	Step	Abs. Error	PDE Error	Rel. Error	PDE Error ($\times 10^{-2}$)
PhysInstruct		1	0.49%	0.22	8.64%	1.45
DiffusionPDE		2000	7.71%	1.68	13.34%	9.14
CoCoGen		2000	7.44%	1.59	13.17%	7.10
PIDM		2000	9.83%	1.76	17.48%	7.69

There are several promising directions for future work. First, it would be valuable to combine Phys-Instruct with more advanced distillation techniques, such as SIM (Luo et al., 2024b) and Uni-Instruct (Wang et al., 2025), to better transfer the knowledge from the teacher while improving the diversity of the student-generated samples. Second, for conditional problems, lightweight adaptation mechanisms (e.g., adapters (Mou et al., 2024) or LoRA (Hu et al., 2022)) could offer a parameter-efficient alternative to full conditional models on top of the pretrained Phys-Instruct priors. Finally, extending Phys-Instruct to higher-dimensional PDEs and to resolution-robust or resolution-free settings (Yao et al., 2025) is an important next step toward practical scientific applications. We hope Phys-Instruct provides a useful foundation for building efficient physics-aware generative models for PDE solving.

Impact Statement

This work aims to advance the fundamental state of Machine Learning. While the advancement of the field generally carries potential societal consequences, this specific work does not present unique ethical or societal issues that require separate highlight.

References

Giacomo Baldan, Qiang Liu, Alberto Guardone, and Nils Thuerey. Flow matching meets pdes: A unified framework for physics-constrained generation. *arXiv preprint arXiv:2506.08604*, 2025. URL <https://arxiv.org/abs/2506.08604>.

Lorenzo Baldassari, Ali Siahkoohi, Josselin Garnier, Knut Solna, and Maarten V de Hoop. Conditional score-based diffusion models for Bayesian inference in infinite dimensions. In *Advances in Neural Information Processing Systems*, volume 36, 2023. URL <https://openreview.net/forum?id=voG6nEW9BV>.

Jan-Hendrik Bastek, WaiChing Sun, and Dennis M Kochmann. Physics-informed diffusion models. In *International Conference on Learning Representations (ICLR)*, 2025.

Shengze Cai, Zhiping Mao, Zhicheng Wang, Minglang Yin, and George Em Karniadakis. Physics-Informed Neural Networks (PINNs) for Fluid Mechanics: A Review. *Acta Mechanica Sinica*, 37(12): 1727–1738, 2021.

Hyungjin Chung, Jeongsol Kim, Michael T Mccann, Marc L Klasky, and Jong Chul Ye. Diffusion posterior sampling for general noisy inverse problems. In *The Eleventh International Conference on Learning Representations*, 2023. URL <https://openreview.net/forum?id=OnD9zGAGT0k>.

Giannis Daras, Hyungjin Chung, Chieh-Hsin Lai, Yuki Mitsufuji, Jong Chul Ye, Peyman Milanfar, Alexandros G. Dimakis, and Mauricio Delbracio. A survey on diffusion models for inverse problems, 2024. URL <https://arxiv.org/abs/2410.00083>.

Agnimitra Dasgupta, Harisankar Ramaswamy, Javier Murgotio-Esandi, Ken Foo, Runze Li, Qifa Zhou, Brendan F. Kennedy, and Assad A. Oberai. Conditional score-based diffusion models for solving inverse elasticity problems. *Computer Methods in Applied Mechanics and Engineering*, 433:117425, 2025. doi: 10.1016/j.cma.2024.117425. URL <https://www.sciencedirect.com/science/article/pii/S0045782524006807>.

Tim Dockhorn, Arash Vahdat, and Karsten Kreis. GENIE: Higher-order denoising diffusion solvers. In *Advances in Neural Information Processing Systems*, volume 35, pages 30150–30166, 2022.

Ying Fan, Olivia Watkins, Yuqing Du, Hao Liu, Moonkyung Ryu, Craig Boutilier, Pieter Abbeel, Mohammad Ghavamzadeh, Kangwook Lee, and Kimin Lee. DPOK: Reinforcement Learning for Fine-Tuning Text-to-Image Diffusion Models. *Advances in Neural Information Processing Systems (NeurIPS)*, 36:79858–79885, 2023.

Zhengyang Geng, Mingyang Deng, Xingjian Bai, J. Zico Kolter, and Kaiming He. Mean Flows for One-Step Generative Modeling. *arXiv preprint arXiv:2505.13447*, 2025a.

Zhengyang Geng, Ashwini Pokle, Weijian Luo, Justin Lin, and J. Zico Kolter. Consistency Models Made Easy. In *Proc. of the International Conference on Learning Representation (ICLR)*. OpenReview.net, 2025b.

Jonathan Ho, Ajay Jain, and Pieter Abbeel. Denoising diffusion probabilistic models. In *Advances in Neural Information Processing Systems*, volume 33, pages 6840–6851, 2020. URL <https://proceedings.neurips.cc/paper/2020/file/4c5bcfec8584af0d967f1ab10179ca4b-Paper.pdf>.

Edward J Hu, Yelong Shen, Phillip Wallis, Zeyuan Allen-Zhu, Yuanzhi Li, Shean Wang, Lu Wang, and Weizhu Chen. Lora: Low-rank adaptation of large language models. In *International Conference on Learning Representations (ICLR)*, 2022.

Jiahe Huang, Guandao Yang, Zichen Wang, and Jeong Joon Park. Diffusionpde: Generative pde-solving under partial observation. In *Advances in Neural Information Processing Systems*, volume 37, 2024a.

Zemin Huang, Zhengyang Geng, Weijian Luo, and Guo-jun Qi. Flow generator matching. *arXiv preprint arXiv:2410.19310*, 2024b.

Christian Jacobsen, Yilin Zhuang, and Karthik Duraisamy. Cocogen: Physically consistent and conditioned score-based generative models for forward and inverse problems. *SIAM Journal on Scientific Computing*, 2024. doi: 10.1137/24M1636071.

Tero Karras, Miika Aittala, Timo Aila, and Samuli Laine. Elucidating the design space of diffusion-based generative models. In *Proceedings of the 36th Conference on Neural Information Processing Systems (NeurIPS 2022)*, 2022.

Dongjun Kim, Chieh-Hsin Lai, Wei-Hsiang Liao, Naoki Murata, Yuhta Takida, Toshimitsu Uesaka, Yutong He, Yuki Mitsufuji, and Stefano Ermon. Consistency Trajectory Models: Learning Probability Flow ODE Trajectory of Diffusion. In *Proc. of the International Conference on Learning Representation (ICLR)*, 2024.

Soheil Kolouri, Kimia Nadjahi, Umut Simsekli, Roland Badeau, and Gustavo K Rohde. Generalized sliced wasserstein distances. In *Advances in Neural Information Processing Systems (NeurIPS)*, volume 32, 2019.

Zongyi Li, Nikola Kovachki, Kamyar Azizzadenesheli, Burigede Liu, Kaushik Bhattacharya, Andrew Stuart, and Anima Anandkumar. Fourier neural operator for parametric partial differential equations. In *International Conference on Learning Representations*, 2021. URL <https://openreview.net/forum?id=c8aUC5b6fPi>.

Xingchao Liu, Chengyue Gong, and Qiang Liu. Flow straight and fast: Learning to generate and transfer data with rectified flow. In *International Conference on Learning Representations (ICLR)*, 2023. URL <https://openreview.net/forum?id=Xc99ZMQtrX>.

Cheng Lu and Yang Song. Simplifying, Stabilizing and Scaling Continuous-time Consistency Models. In *Proc. of the International Conference on Learning Representation (ICLR)*. OpenReview.net, 2025.

Cheng Lu, Yuhao Zhou, Fan Bao, Jianfei Chen, Chongxuan Li, and Jun Zhu. Dpm-solver++: Fast solver for guided sampling of diffusion probabilistic models. *arXiv preprint arXiv:2211.01095*, 2022.

Shanchuan Luo, Xiaohui Wang, Fan Zhang, et al. Latent Consistency Models: Synthesizing High-Resolution Images with Few-Step Inference. *arXiv preprint arXiv:2310.04378*, 2023a.

Weijian Luo, Tianyang Hu, Shifeng Zhang, Jiacheng Sun, Zhenguo Li, and Zhihua Zhang. Diff-instruct: A universal approach for transferring knowledge from pre-trained diffusion models. In *Advances in Neural Information Processing Systems*, volume 36, 2023b.

Weijian Luo, Colin Zhang, Debing Zhang, and Zhengyang Geng. Diff-instruct*: Towards human-preferred one-step text-to-image generative models, 2024a. URL <https://arxiv.org/abs/2410.20898>.

Weijian Luo, Ting Zhu, Shifeng Zhang, Zhenguo Li, and Zhihua Zhang. One-Step Diffusion Distillation through Score Implicit Matching. In *Advances in Neural Information Processing Systems (NeurIPS)*, 2024b.

Yihong Luo, Xiaolong Chen, Xinghua Qu, Tianyang Hu, and Jing Tang. You Only Sample Once: Taming One-Step Text-to-Image Synthesis by Self-Cooperative Diffusion GANs. In *Proc. of the International Conference on Learning Representation (ICLR)*. OpenReview.net, 2025a.

Yihong Luo, Tianyang Hu, Weijian Luo, Kenji Kawaguchi, and Jing Tang. Reward-Instruct: A Reward-Centric Approach to Fast Photo-Realistic Image Generation. *arXiv preprint arxiv.org/abs/2503.13070*, 2025b.

Chong Mou, Xintao Wang, Liangbin Xie, Yanze Wu, Jian Zhang, Zhongang Qi, Ying Shan, and Xiaohu Qie. T2i-adapter: Learning adapters to dig out more controllable ability for text-to-image diffusion models. In *Proceedings of the AAAI Conference on Artificial Intelligence*, volume 38, pages 4296–4304, 2024.

Alexander Quinn Nichol and Prafulla Dhariwal. Improved denoising diffusion probabilistic models. In *Proceedings of the 38th International Conference on Machine Learning*, pages 8162–8171. PMLR, 2021.

Maziar Raissi, Paris Perdikaris, and George E Karniadakis. Physics-Informed Neural Networks: A Deep Learning Framework for Solving Forward and Inverse Problems Involving Nonlinear Partial Differential Equations. *Journal of Computational Physics*, 378:686–707, 2019.

Tim Salimans and Jonathan Ho. Progressive distillation for fast sampling of diffusion models. In *International Conference on Learning Representations (ICLR)*, 2022. URL <https://openreview.net/forum?id=TIdIXIpzhoI>.

Andy Shih, Suneel Belkhale, Stefano Ermon, Dorsa Sadigh, and Nima Anari. Parallel sampling of diffusion models. In *Advances in Neural Information Processing Systems*, volume 36, pages 56403–56430, 2023.

Dule Shu, Zijie Li, and Amir Barati Farimani. A physics-informed diffusion model for high-fidelity flow field reconstruction. *Journal of Computational Physics*, 478:111972, 2023. doi: 10.1016/j.jcp.2023.111972.

Aliaksandra Shysheya, Cristiana Diaconu, Federico Bergamin, Paris Perdikaris, José Miguel Hernández-Lobato, Richard E Turner, and Emile Mathieu. On conditional diffusion models for PDE simulations. In *Advances in Neural Information Processing Systems*, volume 37, 2024. URL <https://openreview.net/forum?id=nQl8EjyMzh>.

Yang Song and Prafulla Dhariwal. Improved Techniques for Training Consistency Models. In *Proc. of the International Conference on Learning Representation (ICLR)*. OpenReview.net, 2024.

Yang Song and Stefano Ermon. Generative modeling by estimating gradients of the data distribution. In *Advances in Neural Information Processing Systems*, volume 32, pages 11895–11907, 2019. URL <https://proceedings.neurips.cc/paper/2019/file/3001ef257407d5a371a96dc947c7d93-Paper.pdf>.

Yang Song, Jascha Sohl-Dickstein, Diederik P. Kingma, Abhishek Kumar, Stefano Ermon, and Ben Poole. Score-based generative modeling through stochastic differential equations. In *Proceedings of the International Conference on Learning Representations (ICLR) 2021*, 2021.

Yang Song, Prafulla Dhariwal, Mark Chen, and Ilya Sutskever. Consistency models. In *Proceedings of the 40th International Conference on Machine Learning*, volume 202 of *Proceedings of Machine Learning Research*, pages 32211–32252. PMLR, 2023. URL <https://proceedings.mlr.press/v202/song23a.html>.

Danica J Sutherland, Hsiao-Yu Tung, Heiko Strathmann, Soumyajit De, Aaditya Ramdas, Alex Smola, and Arthur Gretton. Generative models and model criticism via optimized maximum mean discrepancy. In *International Conference on Learning Representations (ICLR)*, 2017.

Ting Wang, Petr Plecháč, and Jaroslaw Knap. Generative diffusion learning for parametric partial differential equations, 2023. URL <https://arxiv.org/abs/2305.14703>.

Yifei Wang, Weimin Bai, Colin Zhang, Debing Zhang, Weijian Luo, and He Sun. Uni-Instruct: One-step Diffusion Model through Unified Diffusion Divergence Instruction. *arXiv preprint arXiv:2505.20755*, 2025.

Jiqing Wu, Zhiwu Huang, Dinesh Acharya, Wen Li, Janine Thoma, Danda Pani Paudel, and Luc Van Gool. Sliced wasserstein generative models. In *Proceedings of the IEEE/CVF Conference on Computer Vision and Pattern Recognition (CVPR)*, pages 3713–3722, 2019.

Sirui Xie, Zhisheng Xiao, Diederik P. Kingma, Tingbo Hou, Ying Nian Wu, Kevin P. Murphy, Tim Salimans, Ben Poole, and Ruiqi Gao. EM Distillation for One-step Diffusion Models. In *Advances in Neural Information Processing Systems (NeurIPS)*, 2024.

Yilun Xu, Weili Nie, and Arash Vahdat. One-step Diffusion Models with f -Divergence Distribution Matching. *arXiv preprint arXiv:2502.15681*, 2025.

Gefan Yang and Stefan Sommer. A denoising diffusion model for fluid field prediction, 2023.

Jiachen Yao, Abbas Mammadov, Julius Berner, Gavin Kerrigan, Jong Chul Ye, Kamyar Azizzadenesheli, and Anima Anandkumar. Guided diffusion sampling on function spaces with applications to pdes, 2025. URL <https://arxiv.org/abs/2505.17004>. arXiv:2505.17004v2.

Tianwei Yin, Michaël Gharbi, Taesung Park, Richard Zhang, Eli Shechtman, Frédo Durand, and Bill Freeman. Improved Distribution Matching Distillation for Fast Image Synthesis. In *Advances in Neural Information Processing Systems (NeurIPS)*, 2024a.

Tianwei Yin, Michaël Gharbi, Richard Zhang, Eli Shechtman, Frédo Durand, William T. Freeman, and Taesung Park. One-Step Diffusion with Distribution Matching Distillation. In *The IEEE Conference on Computer Vision and Pattern Recognition (CVPR)*, 2024b.

Mingze Yuan, Pengfei Jin, Na Li, and Quanzheng Li. Pirf: Physics-informed reward fine-tuning for diffusion models, 2025.

Lvmin Zhang, Anyi Rao, and Maneesh Agrawala. Adding conditional control to text-to-image diffusion models. In *Proceedings of the IEEE/CVF International Conference on Computer Vision (ICCV)*, pages 3836–3847, 2023.

Yi Zhang and Difan Zou. Physics-informed distillation of diffusion models for pde-constrained generation, 2025. URL <https://arxiv.org/abs/2505.22391>.

Haoyang Zheng and Guang Lin. Muti-Fidelity Prediction and Uncertainty Quantification with Laplace Neural Operators for Parametric Partial Differential Equations. *arXiv preprint arXiv:2502.00550*, 2025a.

Haoyang Zheng and Guang Lin. LES-SINDy: Laplace-Enhanced Sparse Identification of Nonlinear Dynamical Systems. *Journal of Computational Physics*, page 114443, 2025b.

Haoyang Zheng, Jeffrey R Petrella, P Murali Doraiswamy, Guang Lin, Wenrui Hao, and Alzheimer’s Disease Neuroimaging Initiative. Data-Driven Causal Model Discovery and Personalized Prediction in Alzheimer’s Disease. *NPJ Digital Medicine*, 5(1):137, 2022.

Haoyang Zheng, Yao Huang, Ziyang Huang, Wenrui Hao, and Guang Lin. HomPINNs: Homotopy Physics-Informed Neural Networks for Solving the Inverse Problems of Nonlinear Differential Equations with Multiple Solutions. *Journal of Computational Physics*, 500:112751, 2024.

Haoyang Zheng, Xinyang Liu, Cindy Xiangrui Kong, Nan Jiang, Zheyuan Hu, Weijian Luo, Wei Deng, and Guang Lin. Ultra-fast language generation via discrete diffusion divergence instruct. *arXiv preprint arXiv:2509.25035*, 2025a.

Hongkai Zheng, Wenda Chu, Bingliang Zhang, Zihui Wu, Austin Wang, Berthy T. Feng, Caifeng Zou, Yu Sun, Nikola Kovachki, Zachary E. Ross, Katherine L. Bouman, and Yisong Yue. Inversebench: Benchmarking plug-and-play diffusion priors for inverse problems in physical sciences. In *International Conference on Learning Representations (ICLR)*, 2025b. URL <https://openreview.net/forum?id=U3PBIXNG6>.

Mingyuan Zhou, Huangjie Zheng, Zhendong Wang, Mingzhang Yin, and Hai Huang. Score Identity Distillation: Exponentially Fast Distillation of Pretrained Diffusion Models for One-Step Generation. In *Proc. of the International Conference on Machine Learning (ICML)*. OpenReview.net, 2024a.

Zhenyu Zhou, Defang Chen, Can Wang, and Chun Chen. Fast ODE-based sampling for diffusion models in around 5 steps. In *Proceedings of the IEEE/CVF Conference on Computer Vision and Pattern Recognition*, pages 7777–7786, 2024b.

Contents

1	Introduction	1
2	Related Work	3
2.1	Diffusion priors for PDE fields.	3
2.2	Few-step diffusion and distillation.	3
3	Background	3
3.1	Problem Setup of PDE Solvers	3
3.2	Diffusion Models	4
3.3	Integral Kullback-Leibler Divergence	4
4	Phys-Instruct	5
4.1	Phys-Instruct Generator	5
4.2	PDE Error and Physics Loss.	6
4.3	Phys-Instruct Objective	6
4.4	Training Procedure	8
5	Experiments	8
5.1	Main Results	10
5.2	Ablation Studies	11
5.3	Downstream tasks	11
6	Conclusion and Future Work	12
A	PDE Benchmark Details	19
A.1	Darcy Flow	19
A.2	Poisson Equation	20
A.3	Inhomogeneous Helmholtz Equation	20
A.4	Non-bounded Navier–Stokes Equation	20
A.5	Burgers’ Equation	21
B	Proof of Theorem 4.1	21
C	Additional Distributional Metrics	23
D	Extra Ablation Studies	24
D.1	Sensitivity to the physics guidance weight λ_{phys}	24
D.2	Sensitivity to the initial noise level σ_{init}	25
D.3	Ablation on step operator	25
E	Conditional Downstream Tasks with ControlNet	26
F	Extra Results	28
F.1	Qualitative results of Darcy flow	28
F.2	Helmholtz forward problem	28
F.3	Additional forward problem	28
F.4	Additional reconstruction problem	28

A. PDE Benchmark Details

This section provides benchmark details for the five PDEs used in our experiments. A PDE sample is denoted by $\mathbf{x} = (\mathbf{a}, \mathbf{u})$, where \mathbf{a} collects coefficient/forcing/initial-condition fields and \mathbf{u} is the corresponding solution field or the target solution state for dynamic problems.

For each benchmark, all fields are represented on a fixed grid $\mathcal{D}_h = \{\xi_i\}_{i=1}^N \subset \Omega$. For static problems on $\Omega_x \subset \mathbb{R}^d$, we take $\xi = \mathbf{c} \in \Omega_x$ and $\mathcal{D}_h = \{\mathbf{c}_i\}_{i=1}^{N_x}$. For dynamic problems on $\Omega = \Omega_x \times \Omega_t$, we use the space-time coordinate $\xi = (\mathbf{c}, \tau)^\top$ and a tensor grid $\mathcal{D}_h = \{(\mathbf{c}_i, \tau_j)\}_{i=1, j=1}^{N_x, N_t}$. Following [Huang et al. \(2024a\)](#), we generate 50,000 samples as training data and 20,000 as test data per PDE. Darcy flow coefficient fields are drawn from Gaussian random fields (GRFs), and solutions are computed by solving the resulting sparse grid-discretized elliptic system. Non-bounded Navier–Stokes data follow the FNO benchmark data-generation pipeline and FEM solvers ([Li et al., 2021](#)). Poisson and inhomogeneous Helmholtz data are generated using second-order finite-difference schemes, and Burgers’ data follow [Zheng and Lin \(2025a,b\)](#) with a spectral solver to produce space–time fields. All fields are stored as discretized arrays on the target grids.

On the same grid \mathcal{D}_h , we follow Section 4.2 to compute the benchmark physics penalty: $r(\mathbf{x})_i := \mathcal{G}_h[\mathbf{x}](\xi_i)$ and $\mathcal{R}(\mathbf{x})$ is given by (6). When boundary values are prescribed, we enforce them explicitly and evaluate $\mathcal{R}(\mathbf{x})$ only on interior (unconstrained) nodes to avoid boundary-discretization artifacts. The explicit form of \mathcal{G}_h (and thus $\mathcal{R}(\mathbf{x})$) is benchmark-dependent and will be specified for each PDE below.

The PDE datasets are used to learn the data distribution p_0 by training the multi-step diffusion *teacher* score model s_ν , which is then frozen, and to construct evaluation/conditional test instances. In contrast, student distillation does not require paired ground-truth supervision: during distillation, clean samples are generated on-the-fly as $\mathbf{x}_0 = g_\theta(\mathbf{z}; k)$, and physics guidance is applied by evaluating the PDE error penalty $\mathcal{R}(\mathbf{x}_0)$ on these samples.

A.1. Darcy Flow

We consider the static Darcy flow on $\Omega_x = (0, 1)^2$ with homogeneous Dirichlet boundary:

$$\begin{cases} -\nabla \cdot (\mathbf{a}(\mathbf{c}) \nabla u(\mathbf{c})) = q(\mathbf{c}), & \mathbf{c} \in \Omega_x, \\ u(\mathbf{c}) = 0, & \mathbf{c} \in \partial\Omega_x, \end{cases} \quad (11)$$

where the forcing is fixed as $q(\mathbf{c}) \equiv 1$.

Each dataset sample is obtained by first drawing a random permeability field and then solving the PDE. Following DiffusionPDE [Huang et al. \(2024a\)](#), we construct heterogeneous coefficients from a Gaussian random field sampled on the target grid. Specifically, we draw a zero-mean GRF on a 32×32 grid (using a Gaussian-correlated spectral sampler) and define a binary-valued permeability by pointwise thresholding:

$$\mathbf{a}_{ij} = \begin{cases} 12, & \mathbf{m}_{ij} \geq 0, \\ 3, & \mathbf{m}_{ij} < 0, \end{cases} \quad (i, j) \in \mathcal{D}_h,$$

where $\mathbf{m} \in \mathbb{R}^{32 \times 32}$ denotes the sampled GRF and \mathcal{D}_h is the uniform grid over Ω_x . Given \mathbf{a} , we solve the corresponding discretized Darcy system with homogeneous Dirichlet boundary conditions, and store the resulting fields on the same 32×32 grid.

We denote the discretized fields by boldface symbols: $\mathbf{a} \in \mathbb{R}^{32 \times 32}$ and $\mathbf{u} \in \mathbb{R}^{32 \times 32}$ are the grid-sampled permeability and solution fields, respectively. Thus, each sample is $\mathbf{x} = (\mathbf{a}, \mathbf{u})$, where \mathbf{a} specifies the PDE instance and \mathbf{u} is its solution.

For a discrete sample $\mathbf{x} = (\mathbf{a}, \mathbf{u})$ on $\mathcal{D}_h \subset \Omega_x$, we define the interior PDE error:

$$r_{\text{Darcy}}(\mathbf{x})_i := -(\nabla_h \cdot (\mathbf{a} \nabla_h \mathbf{u}))_i - q_i, \quad i \in \mathcal{I}_{\text{int}}, \quad (12)$$

where ∇_h and $\nabla_h \cdot$ are the discrete gradient/divergence operators consistent with the data-generation discretization, and \mathcal{I}_{int} denotes interior grid nodes.

A.2. Poisson Equation

We consider the static Poisson equation on $\Omega_x = (0, 1)^2$ with homogeneous Dirichlet boundary:

$$\begin{cases} \nabla^2 u(\mathbf{c}) = a(\mathbf{c}), & \mathbf{c} \in \Omega_x, \\ u(\mathbf{c}) = 0, & \mathbf{c} \in \partial\Omega_x. \end{cases} \quad (13)$$

Each dataset sample is generated by first drawing a random forcing field and then solving the PDE. Following [Huang et al. \(2024a\)](#), we set $a = \mu$ where μ is sampled from the Gaussian random field. We solve for u using a second-order finite-difference scheme, enforcing the homogeneous Dirichlet boundary via the standard mollifier $\sin(\pi c_1) \sin(\pi c_2)$ in the data-generation pipeline. We store the discretized fields on a 32×32 grid and denote each sample by $\mathbf{x} = (\mathbf{a}, \mathbf{u})$.

On $\mathcal{D}_h \subset \Omega_x$, we evaluate the benchmark-consistent discrete PDE error map \mathcal{G}_h using the second-order Laplacian, yielding the interior PDE error

$$r_{\text{Pois}}(\mathbf{x})_i := (\Delta_h \mathbf{u})_i - \mathbf{a}_i, \quad i \in \mathcal{I}_{\text{int}}, \quad (14)$$

where Δ_h is the standard second-order discrete Laplacian on the uniform grid.

A.3. Inhomogeneous Helmholtz Equation

We consider the static inhomogeneous Helmholtz equation on $\Omega_x = (0, 1)^2$ with homogeneous Dirichlet boundary:

$$\begin{cases} \nabla^2 u(\mathbf{c}) + k^2 u(\mathbf{c}) = a(\mathbf{c}), & \mathbf{c} \in \Omega_x, \\ u(\mathbf{c}) = 0, & \mathbf{c} \in \partial\Omega_x, \end{cases} \quad (15)$$

where we set $k = 1$ (note that this reduces to the Poisson equation when $k = 0$).

This benchmark follows the same generation pipeline as Poisson and we store each sample $\mathbf{x} = (\mathbf{a}, \mathbf{u})$ on a 128×128 grid.

Accordingly, the discrete PDE error differs from Poisson only by the additional reaction term:

$$r_{\text{Helm}}(\mathbf{x})_i := (\Delta_h \mathbf{u})_i + k^2 \mathbf{u}_i - \mathbf{a}_i, \quad i \in \mathcal{I}_{\text{int}}, \quad (16)$$

with the same Δ_h as above.

A.4. Non-bounded Navier–Stokes Equation

We study the 2D incompressible Navier–Stokes benchmark on $\Omega_x = (0, 1)^2$ with periodic (non-bounded) boundary conditions in the vorticity formulation:

$$\begin{cases} \partial_\tau \omega(\mathbf{c}, \tau) + \mathbf{v}(\mathbf{c}, \tau) \cdot \nabla \omega(\mathbf{c}, \tau) = \nu \Delta \omega(\mathbf{c}, \tau) + q(\mathbf{c}), & (\mathbf{c}, \tau) \in \Omega_x \times (0, T], \\ \nabla \cdot \mathbf{v}(\mathbf{c}, \tau) = 0, & (\mathbf{c}, \tau) \in \Omega_x \times (0, T], \end{cases} \quad (17)$$

where $\nu = 10^{-3}$, and $\omega = \nabla \times \mathbf{v}$ is the scalar vorticity. The forcing follows the fixed pattern

$$q(\mathbf{c}) = \frac{1}{10} \left(\sin(2\pi(c_1 + c_2)) + \cos(2\pi(c_1 + c_2)) \right). \quad (18)$$

Following [Huang et al. \(2024a\)](#), the initial condition is sampled from a Gaussian random field

$$\omega_0 \sim \mathcal{N}(0, 7^{1.5}(-\Delta + 49\mathbf{I})^{-2.5}). \quad (19)$$

Given ω_0 and the fixed forcing q , we solve the dynamics using a pseudo-spectral method in the stream-function formulation: we advance the vorticity equation in the Fourier domain and evaluate nonlinear terms in physical space via inverse FFTs. We simulate for 1 second using 10 time steps. In the dataset convention of DiffusionPDE, we take the terminal snapshot index as $T = 10$. We store (ω_0, ω_T) on a 64×64 spatial grid and denote the resulting discrete sample by $\mathbf{x} = (\omega_0, \omega_T)$, i.e., $\mathbf{a} = \omega_0$ and $\mathbf{u} = \omega_T$, yielding resolution $64 \times 64 \times 2$.

As in [Huang et al. \(2024a\)](#), since T is large in the benchmark convention, we do not evaluate the full time-dependent PDE error at the terminal state. Instead, we adopt a simplified terminal-time constraint evaluated directly on the predicted vorticity snapshot and define

$$r_{\text{NS}}(\mathbf{x})_{i,j} := (\partial_{x,h}\omega_T)_{i,j} + (\partial_{y,h}\omega_T)_{i,j}, \quad (i, j) \in \mathcal{I}_{\text{all}}, \quad (20)$$

where $\partial_{x,h}$ and $\partial_{y,h}$ are central differences.

A.5. Burgers' Equation

We consider the 1D viscous Burgers' equation on $\Omega_x = (0, 1)$ with periodic boundary conditions:

$$\begin{cases} \partial_\tau u(c, \tau) + \partial_c \left(\frac{u(c, \tau)^2}{2} \right) - \nu \partial_{cc} u(c, \tau) = 0, & (c, \tau) \in \Omega_x \times (0, T], \\ u(c, 0) = u_0(c), & c \in \Omega_x, \end{cases} \quad (21)$$

where $\nu = 0.01$, we take the physical simulation horizon $T = 1$, and enforce periodicity in space (e.g., $u(0, \tau) = u(1, \tau)$ for all $\tau \in (0, T]$).

Following [Huang et al. \(2024a\)](#) and the FNO benchmark procedure, the initial condition is sampled as a Gaussian random field

$$u_0 \sim \mathcal{N}(0, 625(-\Delta + 25\mathbf{I})^{-2}). \quad (22)$$

Given u_0 , we solve the PDE using a spectral method and simulate over $t \in [0, 1]$ with 128 uniformly spaced time snapshots (including $t = 0$), producing a space-time solution field $u_{0:T}$. We store $\mathbf{u} = u_{0:T}$ on a 128×128 tensor grid over (c, τ) .

Since the time dimension is densely discretized, we compute the pointwise PDE error by finite differences:

$$r_{\text{Burg}}(\mathbf{x})_{i,j} := (\partial_{\tau,h}\mathbf{u})_{i,j} + (\partial_{c,h}(\frac{1}{2}\mathbf{u}^2))_{i,j} - \nu (\partial_{cc,h}\mathbf{u})_{i,j}, \quad (i, j) \in \mathcal{I}_{\text{all}}, \quad (23)$$

where $\partial_{\tau,h}$, $\partial_{c,h}$ and $\partial_{cc,h}$ are standard discrete operators with periodic wrapping in space.

B. Proof of Theorem 4.1

Proof of Theorem 4.1. We first justify the penalized objective used in the analysis. The constrained formulation (7) is not optimized directly in our implementation. Instead, we adopt a penalty relaxation

and treat $\lambda_{\text{phys}} > 0$ as a trade-off hyperparameter, which augments the IKL matching term by a soft penalty on the constraint violation. Concretely, consider the Lagrangian-type surrogate

$$\mathcal{D}_{\text{IKL}}^{[0,T]}(q_\theta \| p) + \lambda_{\text{phys}} \left(\mathbb{E}_{\mathbf{x}_0 \sim q_\theta} [\mathcal{R}(\mathbf{x}_0)] - \varepsilon \right).$$

Since $-\lambda_{\text{phys}}\varepsilon$ is a constant independent of θ , it does not affect the gradient with respect to θ and can be dropped. Moreover, under our unified k -step generator parameterization, a clean student sample satisfies $\mathbf{x}_0 = g_\theta(\mathbf{z}; k)$ with $\mathbf{z} \sim p_{\mathbf{z}}$ and $k \sim \Delta_K$, which induces the implicit distribution q_θ . Therefore,

$$\mathbb{E}_{\mathbf{x}_0 \sim q_\theta} [\mathcal{R}(\mathbf{x}_0)] = \mathbb{E}_{\mathbf{z} \sim p_{\mathbf{z}}, k \sim \Delta_K, \mathbf{x}_0 = g_\theta(\mathbf{z}; k)} [\mathcal{R}(\mathbf{x}_0)].$$

Combining the above yields the implemented penalized objective

$$\mathcal{L}_G(\theta) = \mathcal{D}_{\text{IKL}}^{[0,T]}(q_\theta \| p) + \lambda_{\text{phys}} \mathbb{E}_{\mathbf{z} \sim p_{\mathbf{z}}, k \sim \Delta_K, \mathbf{x}_0 = g_\theta(\mathbf{z}; k)} [\mathcal{R}(\mathbf{x}_0)],$$

which is exactly the objective optimized by the guided generator update.

Throughout, we assume mild regularity so that differentiation can be interchanged with the time integral and expectations, and the sampling procedure that generates $\mathbf{x}_t \sim p_{0t}(\cdot | \mathbf{x}_0)$ admits a pathwise derivative with respect to \mathbf{x}_0 (and thus with respect to θ through $\mathbf{x}_0 = g_\theta(\mathbf{z}; k)$). We also work under the ideal score limit in the theorem, i.e., $s_\phi(\mathbf{x}_t, t) = \nabla_{\mathbf{x}_t} \log q_{\theta,t}(\mathbf{x}_t)$ and $s_\nu(\mathbf{x}_t, t) = \nabla_{\mathbf{x}_t} \log p_t(\mathbf{x}_t)$ for a.e. $t \in [0, T]$ and $\mathbf{x}_t \sim q_{\theta,t}$.

Fix $t \in [0, T]$. The time- t KL term is

$$\mathcal{D}_{\text{KL}}(q_{\theta,t} \| p_t) = \mathbb{E}_{\mathbf{x}_t \sim q_{\theta,t}} [\log q_{\theta,t}(\mathbf{x}_t) - \log p_t(\mathbf{x}_t)].$$

By the sampling procedure in (9), \mathbf{x}_t is obtained by drawing $k \sim \Delta_K$, $\mathbf{z} \sim p_{\mathbf{z}}$, setting $\mathbf{x}_0 = g_\theta(\mathbf{z}; k)$, and sampling $\mathbf{x}_t \sim p_{0t}(\cdot | \mathbf{x}_0)$. Under the above regularity, differentiating the KL term along this sampling path yields

$$\nabla_\theta \mathcal{D}_{\text{KL}}(q_{\theta,t} \| p_t) = \mathbb{E} \left[\nabla_\theta \log q_{\theta,t}(\mathbf{x}_t) + (\nabla_{\mathbf{x}_t} \log q_{\theta,t}(\mathbf{x}_t) - \nabla_{\mathbf{x}_t} \log p_t(\mathbf{x}_t))^\top \nabla_\theta \mathbf{x}_t \right], \quad (24)$$

where the expectation is over $k \sim \Delta_K$, $\mathbf{z} \sim p_{\mathbf{z}}$, $\mathbf{x}_0 = g_\theta(\mathbf{z}; k)$, and $\mathbf{x}_t \sim p_{0t}(\cdot | \mathbf{x}_0)$. The first term vanishes by the score identity $\mathbb{E}_{\mathbf{x}_t \sim q_{\theta,t}} [\nabla_\theta \log q_{\theta,t}(\mathbf{x}_t)] = 0$. Therefore,

$$\nabla_\theta \mathcal{D}_{\text{KL}}(q_{\theta,t} \| p_t) = \mathbb{E} \left[(\nabla_{\mathbf{x}_t} \log q_{\theta,t}(\mathbf{x}_t) - \nabla_{\mathbf{x}_t} \log p_t(\mathbf{x}_t))^\top \nabla_\theta \mathbf{x}_t \right]. \quad (25)$$

Recalling $\mathcal{D}_{\text{IKL}}^{[0,T]}(q_\theta \| p) = \int_0^T w(t) \mathcal{D}_{\text{KL}}(q_{\theta,t} \| p_t) dt$ and interchanging ∇_θ with the integral, we obtain

$$\nabla_\theta \mathcal{D}_{\text{IKL}}^{[0,T]}(q_\theta \| p) = \int_0^T w(t) \mathbb{E} \left[(\nabla_{\mathbf{x}_t} \log q_{\theta,t}(\mathbf{x}_t) - \nabla_{\mathbf{x}_t} \log p_t(\mathbf{x}_t))^\top \nabla_\theta \mathbf{x}_t \right] dt. \quad (26)$$

Under the ideal score limit, $\nabla_{\mathbf{x}_t} \log q_{\theta,t}(\mathbf{x}_t) = s_\phi(\mathbf{x}_t, t)$ and $\nabla_{\mathbf{x}_t} \log p_t(\mathbf{x}_t) = s_\nu(\mathbf{x}_t, t)$, so (26) becomes

$$\nabla_\theta \mathcal{D}_{\text{IKL}}^{[0,T]}(q_\theta \| p) = \int_0^T w(t) \mathbb{E} \left[(s_\phi(\mathbf{x}_t, t) - s_\nu(\mathbf{x}_t, t))^\top \nabla_\theta \mathbf{x}_t \right] dt. \quad (27)$$

In the implemented update, the score term is treated as a constant weight with respect to θ , i.e., gradients are stopped through the score evaluations. Equivalently, we may insert the stop-gradient operator $\text{SG}\{\cdot\}$ on the score difference inside the expectation in (27) without changing the resulting

θ -gradient, since the only θ -dependence being differentiated is carried by the pathwise term $\nabla_\theta x_t$. Therefore,

$$\nabla_\theta \mathcal{D}_{\text{IKL}}^{[0,T]}(q_\theta \| p) = \int_0^T w(t) \mathbb{E} \left[\text{SG} \{ s_\phi(\mathbf{x}_t, t) - s_\nu(\mathbf{x}_t, t) \}^\top \nabla_\theta \mathbf{x}_t \right] dt, \quad (28)$$

where the expectation is over $\mathbf{z} \sim p_{\mathbf{z}}$, $k \sim \Delta_K$, $\mathbf{x}_0 = g_\theta(\mathbf{z}; k)$, and $\mathbf{x}_t \sim p_{0t}(\cdot | \mathbf{x}_0)$.

For the physics term, recall from (9) that the penalty enters as $\lambda_{\text{phys}} \mathcal{L}_{\text{phys}}(\theta)$, where

$$\mathcal{L}_{\text{phys}}(\theta) = \mathbb{E}_{\mathbf{z} \sim p_{\mathbf{z}}, k \sim \Delta_K, \mathbf{x}_0 = g_\theta(\mathbf{z}; k)} [\mathcal{R}(\mathbf{x}_0)].$$

Under the same regularity assumptions, the chain rule yields

$$\nabla_\theta \mathcal{L}_{\text{phys}}(\theta) = \mathbb{E}_{\mathbf{z} \sim p_{\mathbf{z}}, k \sim \Delta_K} \left[(\nabla_{\mathbf{x}_0} \mathcal{R}(\mathbf{x}_0))^\top \nabla_\theta g_\theta(\mathbf{z}; k) \right]_{\mathbf{x}_0 = g_\theta(\mathbf{z}; k)}. \quad (29)$$

Combining (28) with (29) gives

$$\begin{aligned} \nabla_\theta \mathcal{L}_G(\theta) &= \int_0^T w(t) \mathbb{E}_{\substack{\mathbf{z} \sim p_{\mathbf{z}}, k \sim \Delta_K \\ \mathbf{x}_0 = g_\theta(\mathbf{z}; k), \mathbf{x}_t \sim p_{0t}(\cdot | \mathbf{x}_0)}} \left[\text{SG} \{ s_\phi(\mathbf{x}_t, t) - s_\nu(\mathbf{x}_t, t) \}^\top \nabla_\theta \mathbf{x}_t \right] dt \\ &\quad + \lambda_{\text{phys}} \mathbb{E}_{\mathbf{z} \sim p_{\mathbf{z}}, k \sim \Delta_K} \left[(\nabla_{\mathbf{x}_0} \mathcal{R}(\mathbf{x}_0))^\top \nabla_\theta g_\theta(\mathbf{z}; k) \right]_{\mathbf{x}_0 = g_\theta(\mathbf{z}; k)}, \end{aligned}$$

which is exactly (10). This completes the proof. \square

C. Additional Distributional Metrics

In addition to PDE Error, we report distributional discrepancy between generated samples and held-out real data using two-sample distances. These metrics quantify how closely the generated fields match the data distribution, complementing physics-consistency evaluations.

Preprocessing and Normalization.

All distances are computed on the same field representation used for evaluation. For multi-field problems (e.g., coefficient–solution pairs), we apply channel-wise standardization using statistics computed from the real data: for each channel c , we transform both real and generated samples by

$$\tilde{\mathbf{x}}^{(c)} = \frac{\mathbf{x}^{(c)} - \mu_{\text{real}}^{(c)}}{\sigma_{\text{real}}^{(c)} + \epsilon}, \quad (30)$$

where $\mu_{\text{real}}^{(c)}$ and $\sigma_{\text{real}}^{(c)}$ are the mean and standard deviation over the real dataset, and ϵ is a small constant. For single-field benchmarks such as Burgers' equation, this reduces to standardization of the scalar field.

Sliced Wasserstein Distance (SWD) (Kolouri et al., 2019; Wu et al., 2019).

Let P and Q denote the empirical distributions of standardized generated and real samples, respectively. SWD approximates the Wasserstein distance in high dimensions by averaging 1D Wasserstein distances over random projections:

$$\text{SWD}(P, Q) = \frac{1}{K} \sum_{k=1}^K W_1(\langle \mathbf{v}_k, \mathbf{x} \rangle_{\mathbf{x} \sim P}, \langle \mathbf{v}_k, \mathbf{x} \rangle_{\mathbf{x} \sim Q}), \quad (31)$$

Table 5 | Sensitivity of training stability to λ_{phys} . All runs use the same setup as **Default** except for different λ_{phys} . We label runs as *Stable* (training completes normally), *Weak* (training completes but yields limited PDE error improvement), *Unstable* (fails early before the PDE error meaningfully decreases), and *Diverged* (mode collapsed, distillation failed).

λ_{phys}	Status
1e-4	Unstable (early failure; PDE error remains high)
5e-4	Stable, but weak improvement
1e-3	Stable
5e-3	Stable
1e-2	Stable
5e-2	Diverged

where $\{\mathbf{v}_k\}_{k=1}^K$ are i.i.d. random unit vectors and $W_1(\cdot, \cdot)$ is the 1D Wasserstein distance computed via sorting. We use a fixed random seed and $K = 512$ random projections, which provides a stable estimate of SWD at a moderate computational cost for high-dimensional fields.

Maximum Mean Discrepancy (MMD) (Sutherland et al., 2017).

We also report MMD with a multi-scale RBF kernel as a complementary two-sample statistic:

$$\text{MMD}^2(P, Q) = \mathbb{E}_{\mathbf{x}, \mathbf{x}' \sim P} [k(\mathbf{x}, \mathbf{x}')] + \mathbb{E}_{\mathbf{y}, \mathbf{y}' \sim Q} [k(\mathbf{y}, \mathbf{y}')] - 2 \mathbb{E}_{\mathbf{x} \sim P, \mathbf{y} \sim Q} [k(\mathbf{x}, \mathbf{y})], \quad (32)$$

with $k(\mathbf{x}, \mathbf{y}) = \exp(-\|\mathbf{x} - \mathbf{y}\|_2^2/(2\sigma^2))$. Bandwidths are selected from the real data using the median pairwise-distance heuristic: we compute $\hat{\sigma}$ as the median of pairwise distances between a random subset of real samples, and use the multi-scale set $\sigma \in \{\hat{\sigma}/4, \hat{\sigma}/2, \hat{\sigma}, 2\hat{\sigma}, 4\hat{\sigma}\}$. We report $\sqrt{\text{MMD}^2}$ for readability.

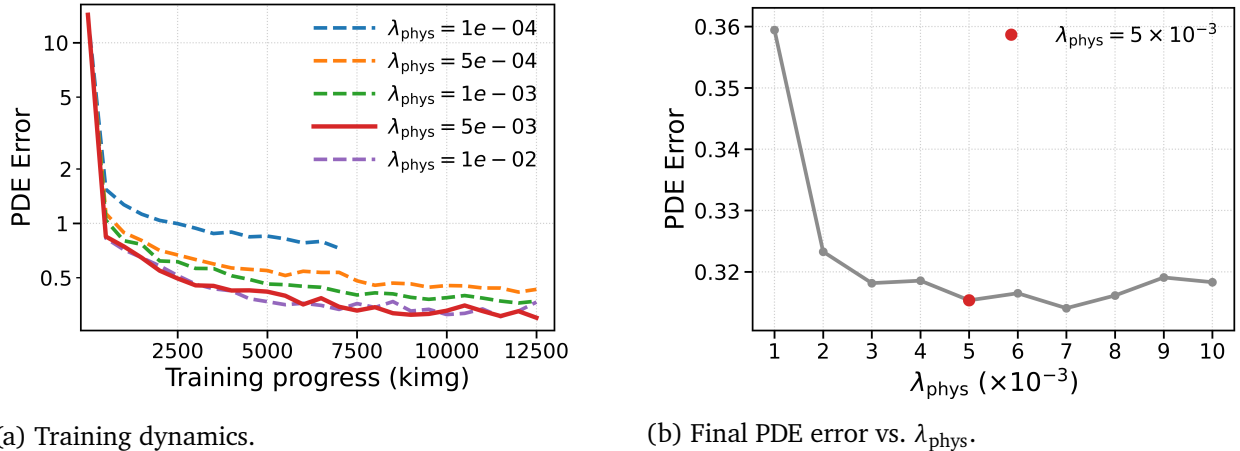
D. Extra Ablation Studies

This appendix provides additional ablations that complement the main-text analysis of physics guidance in one-step Phys-Instruct. Unless otherwise stated, all runs follow the **Default** configuration on Darcy flow, and we report the PDE Error evaluated on one-step samples. Moreover, we also include ablation study of step operator as described in 4.1.

D.1. Sensitivity to the physics guidance weight λ_{phys}

Figure 5 (a) plots the training trajectories of the PDE Error under different physics guidance weights λ_{phys} . Across a broad and practically relevant range, physics guidance consistently accelerates the decay of the PDE error and leads to a lower final plateau. In particular, *moderate* guidance weights yield the most reliable improvements, showing both rapid early reduction and sustained progress throughout training. Figure 5 (b) further summarizes the final PDE error versus λ_{phys} , showing that a moderate range around $5e-3$ achieves the lowest PDE errors.

When λ_{phys} is too small, the physics signal becomes ineffective: training either fails to make meaningful progress or plateaus at a noticeably higher PDE error. Conversely, overly large λ_{phys} can destabilize training and lead to divergence, as summarized in Table 5. These results suggest a *stability-PDE error trade-off*: insufficient weighting under-enforces the PDE constraint, while excessive weighting can dominate the distillation objective and break optimization.



(a) Training dynamics.

(b) Final PDE error vs. λ_{phys} .

Figure 5 | Sensitivity of PDE error to the physics guidance weight λ_{phys} on Darcy flow. (a) We plot PDE error (log scale) versus training progress for one-step Phys-Instruct with different λ_{phys} (all other settings match **Default**). Moderate λ_{phys} yields consistently lower PDE errors, while too small λ_{phys} leads to early instability and a higher error plateau. Diverged runs with overly large λ_{phys} are omitted. (b) Summary of the final PDE error across λ_{phys} with finer grids between $1\text{e-}3$ and $1\text{e-}2$. The red dot denotes the PDE error of default λ_{phys} .

Table 6 | Sensitivity check of the one-step noise level σ_{init} . All settings use the default configuration except for σ_{init} .

σ_{init}	PDE Error ($\times 10^{-1}$) \downarrow
1.00	3.21
1.50 (default)	3.15
3.00	3.18

Overall, the default choice of λ_{phys} lies in a stable regime that achieves strong PDE error reduction without sacrificing training stability, and the method remains robust to moderate variations around this value.

D.2. Sensitivity to the initial noise level σ_{init}

Table 6 studies the sensitivity of one-step Phys-Instruct to the initial noise level σ_{init} , holding all other settings fixed. We find that performance is not highly sensitive to σ_{init} within the tested range: the final PDE Error varies only mildly, indicating that the default σ_{init} is not a fragile tuning choice. This robustness is desirable in practice, as it suggests that one-step distillation with physics guidance does not require aggressive calibration of the initial noise level to achieve good physical consistency.

D.3. Ablation on step operator

Selecting a step operator is equivalent to specifying the few-step generator’s sampling scheme. We use Heun as the default, and additionally report results with an Euler sampler on Darcy flow. As shown in Table 7, switching between Heun and Euler changes Phys-Instruct’s performance only marginally, since both employ a fixed, small-step trajectory.

Table 7 | Unconditional generation results on Darcy flow at resolution $32 \times 32 \times 2$ with two different sampling methods. We report PDE Error \downarrow and the number of sampling steps per sample (Step). The lowest PDE Error within each sampler column is **bolded**.

Method	Step	PDE Error (\downarrow)	
		Euler	Huen
Phys-Instruct	1	3.15×10^{-1}	3.15×10^{-1}
	2	2.31×10^{-1}	2.18×10^{-1}
	3	1.20×10^{-1}	1.35×10^{-1}
	4	8.94×10^{-2}	8.49×10^{-2}

E. Conditional Downstream Tasks with ControlNet

The unconditional Phys-Instruct models learn a prior over PDE fields without paired supervision. In many downstream applications, however, we are given paired data

$$\{(\mathbf{y}_i, \mathbf{x}_i^*)\}_{i=1}^N, \quad (33)$$

where \mathbf{y}_i encodes problem-specific information, such as coefficient fields, boundary conditions, or observation masks, and \mathbf{x}_i^* is the corresponding ground-truth PDE field (solution and, when applicable, coefficients). Conditional Phys-Instruct leverages this supervision while still using the PDE error as physics guidance.

ControlNet-Style Conditional Generator.

We build a conditional generator on top of the unconditional Phys-Instruct backbone,

$$\hat{\mathbf{x}} = g_\theta(\mathbf{z}, \mathbf{y}), \quad \mathbf{z} \sim p_z, \quad (34)$$

where \mathbf{y} provides task-specific conditioning. For conditional downstream tasks, we instantiate g_θ using the one-step Phys-Instruct generator as the backbone, so the explicit sampling step index k is omitted. Our backbones are EDM following the SongUNet architecture (Karras et al., 2022; Song et al., 2021), consisting of an encoder-decoder U-Net with multi-resolution residual blocks and skip connections.

Following Zhang et al. (2023), we attach a *control branch* that processes \mathbf{y} and injects its features into the backbone through zero-initialized residual connections. Let \mathbf{e} denote the shared timestep (noise-level) embedding produced by the mapping network. We first map the condition \mathbf{y} to the channel space of the backbone input \mathbf{z} using a convolutional encoder ψ , and form a condition-augmented input for the control branch:

$$\mathbf{z}^c = \mathbf{z} + \text{ZeroConv}_{\text{in}}(\psi(\mathbf{y})), \quad (35)$$

where $\text{ZeroConv}_{\text{in}}$ is a zero-initialized 1×1 convolution, hence $\mathbf{z}^c \approx \mathbf{z}$ at initialization. The control encoder mirrors the SongUNet encoder (same resolution hierarchy and block layout) and processes $(\mathbf{z}^c, \mathbf{e})$ to produce multi-resolution hints $\{\mathbf{h}_\ell(\mathbf{z}^c, \mathbf{e})\}_\ell$ aligned with the backbone decoder resolutions. Let \mathbf{f}_ℓ denote the backbone feature map immediately before a decoder UNet block at resolution level ℓ . We inject the conditioning by projecting the corresponding hint with a zero-initialized 1×1 convolution Proj_ℓ and adding it to the backbone feature:

$$\mathbf{f}'_\ell = \mathbf{f}_\ell + \text{Proj}_\ell(\mathbf{h}_\ell(\mathbf{z}^c, \mathbf{e})), \quad \mathbf{f}_{\ell, \text{out}} = \text{Block}_\ell(\mathbf{f}'_\ell, \mathbf{e}). \quad (36)$$

Since both $\text{ZeroConv}_{\text{in}}$ and Proj_{ℓ} are zero-initialized, the injected residuals are initially inactive, so the conditional generator starts from the pretrained unconditional behavior and gradually learns to incorporate \mathbf{y} through the residual pathways.

Data Term and Physics Regularization.

For each pair $(\mathbf{y}, \mathbf{x}^*)$ and latent noise \mathbf{z} , the conditional generator produces a prediction

$$\hat{\mathbf{x}} = g_{\theta}(\mathbf{z}, \mathbf{y}).$$

Depending on the task, \mathbf{x}^* may contain full fields or only partially observed components. We write $O_{\mathbf{y}}(\cdot)$ for a generic observation mask that extracts the components of \mathbf{x} that are supervised under condition \mathbf{y} .

The data-fidelity term is then

$$\mathcal{L}_{\text{data}}(\theta) = \mathbb{E}_{(\mathbf{y}, \mathbf{x}^*), \mathbf{z}} \left[\|O_{\mathbf{y}}(\hat{\mathbf{x}}) - O_{\mathbf{y}}(\mathbf{x}^*)\|_2^2 \right]. \quad (37)$$

In addition, we evaluate the PDE error on the full prediction $\hat{\mathbf{x}}$ using the same \mathcal{G}_h as in Sec. 4.2, leading to the same physics error defined in Eq. (8).

Conditional Phys-Instruct Objective.

The Conditional Phys-Instruct generator is trained with a supervised objective regularized by the PDE error:

$$\mathcal{L}_G^{\text{cond}}(\theta) = \mathcal{L}_{\text{data}}(\theta) + \lambda_{\text{phys}} \mathcal{L}_{\text{phys}}(\theta), \quad (38)$$

where $\lambda_{\text{phys}} > 0$ controls the strength of physics guidance.

This formulation allows a pretrained unconditional Phys-Instruct model to be easily and flexibly adapted to handling different downstream conditional tasks by changing the definition of \mathbf{y} and the observation operator $O_{\mathbf{y}}$, while the $\mathcal{L}_{\text{phys}}$ term encourages physically consistent predictions.

Baselines and Metrics.

We compare against DiffusionPDE (Huang et al., 2024a), CoCoGen (Jacobsen et al., 2024), and PIDM (Bastek et al., 2025). All baselines solve conditional tasks via diffusion posterior sampling (DPS), using observation and/or PDE guidance at inference time. DiffusionPDE follows the original design with DPS guidance, CoCoGen appends an additional ten-step PDE-guided refinement after sampling, and PIDM uses the same DPS-style inference as in DiffusionPDE but replaces the backbone with an unconditional PIDM model. We report prediction error (relative L_2 for continuous fields and absolute error for discrete fields) together with PDE Error. Since DPS-based solvers typically require long trajectories to converge, we run baseline inference with Step= 2000 as adopted in Huang et al. (2024a).

Tasks.

We mainly consider three kinds of down stream tasks: (1) Forward problem: inference solution \mathbf{u} from known coefficients \mathbf{a} ; (2) Inverse problem: predict coefficient \mathbf{a} given observed \mathbf{u} ; (3) Reconstruction problem: predict the whole \mathbf{x}^* given its partial observation.

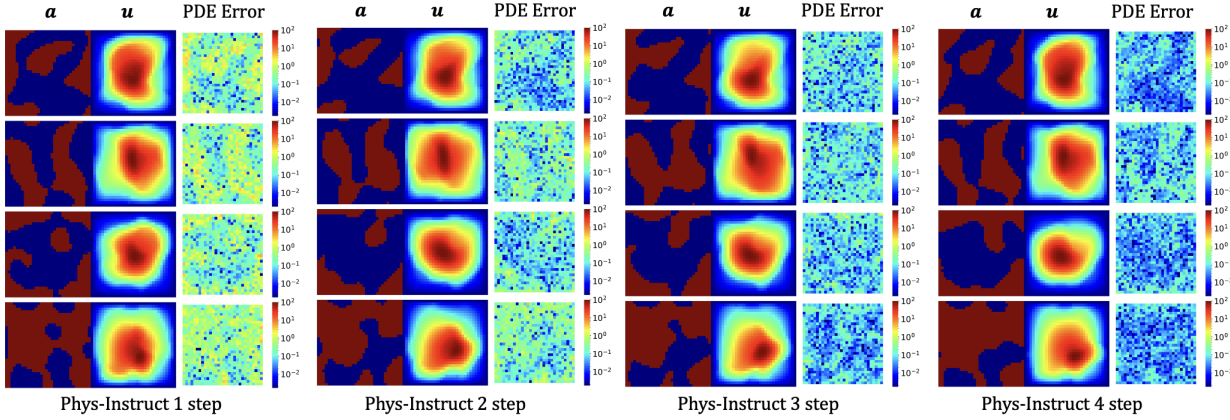


Figure 6 | Phys-Instruct generated Darcy flow samples with 1-4 steps (heun sampler). The PDE error column is showing the absolute value of the PDE error field $r(\mathbf{x})_i$ for every point in the grid.

Table 8 | Forward problems on Darcy flow and Poisson equation. We report relative error and PDE Error (↓). Step denotes the number of sampling steps per sample.

Forward		Darcy Flow		Poisson	
Method	Step	Rel. Error	PDE Error ($\times 10^{-1}$)	Rel. Error	PDE Error ($\times 10^{-1}$)
PhysInstruct	1	0.29%	2.82	2.49%	0.99
DiffusionPDE	2000	4.61%	5.26	7.48%	2.24
CoCoGen	2000	4.39%	4.46	7.25%	2.02
PIDM	2000	7.34%	3.44	5.28%	1.20

F. Extra Results

F.1. Qualitative results of Darcy flow

We show the generated Darcy flow samples under 1-4 steps with Phys-Instruct in Figure 6. With sampling steps increasing, PDE error drops.

F.2. Helmholtz forward problem

Figure 7 shows qualitative comparison of Phys-Instruct with other baseline methods on Helmholtz equation forward problem. It shows that Phys-Instruct achieves low relative error and PDE error with details well captured.

F.3. Additional forward problem

We additionally conducted forward problem on Darcy flow and Poisson equation. We show the results of extra forward problems in Table 8. One step Phys-Instruct achieves lowest relative error on the predicted solution, as well as the lowest PDE error.

F.4. Additional reconstruction problem

We follow Huang et al. (2024a) and consider a Burgers' equation reconstruction setting under sparse observations. Specifically, we randomly sample 5 out of 128 spatial locations as sensors and

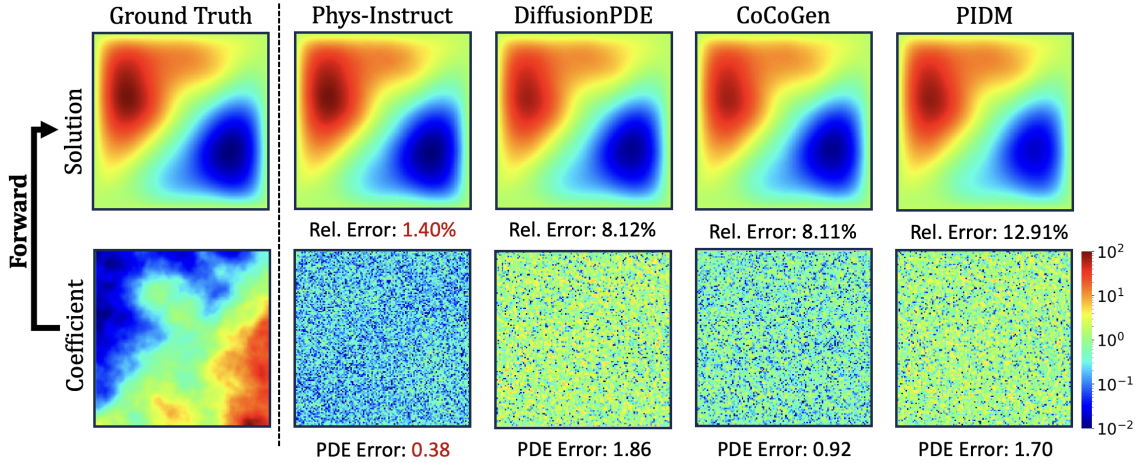


Figure 7 | Qualitative comparison for the Helmholtz forward problem (corresponding to Table 3). The leftmost column shows the ground-truth fields, and the remaining columns show predictions from different methods. The top row visualizes the predicted solution u , and the bottom row shows the pointwise absolute PDE error $|r(\mathbf{x})_i|$ over the grid (log-scaled colorbar). We annotate each method with the solution relative error and the overall PDE Error↓, highlighting that Phys-Instruct achieves the lowest PDE error and best agreement with the ground truth.

Table 9 | Burgers' reconstruction problem. We report relative errors and PDE Error (↓). Step denotes the number of sampling steps per sample.

Method	Step	Partial Observation	
		Rel. Error	PDE Error ($\times 10^{-1}$)
PhysInstruct	1	12.00%	7.59
DiffusionPDE	200	23.96%	9.24
CoCoGen	200	22.81%	8.00
PIDM	200	25.80%	7.91
DiffusionPDE	2000	4.66%	2.42
CoCoGen	2000	4.31%	1.78
PIDM	2000	6.59%	1.62

provide their measurements over time. Given these partial observations, the goal is to recover the full 128×128 spatiotemporal field. Results are summarized in Table 9. We observe an accuracy–latency trade-off: one-step Phys-Instruct improves over baselines using 200 sampling steps in both prediction error and PDE error, while still trailing diffusion baselines with 2000 steps of roll-outs. Nevertheless, as shown in Figure 8, the one-step reconstructions preserves the dominant spatiotemporal patterns of the ground truth, supporting the use of one-step sampling as a low-latency reconstruction baseline, which can serve as a strong initialization for subsequent refinement if desired.

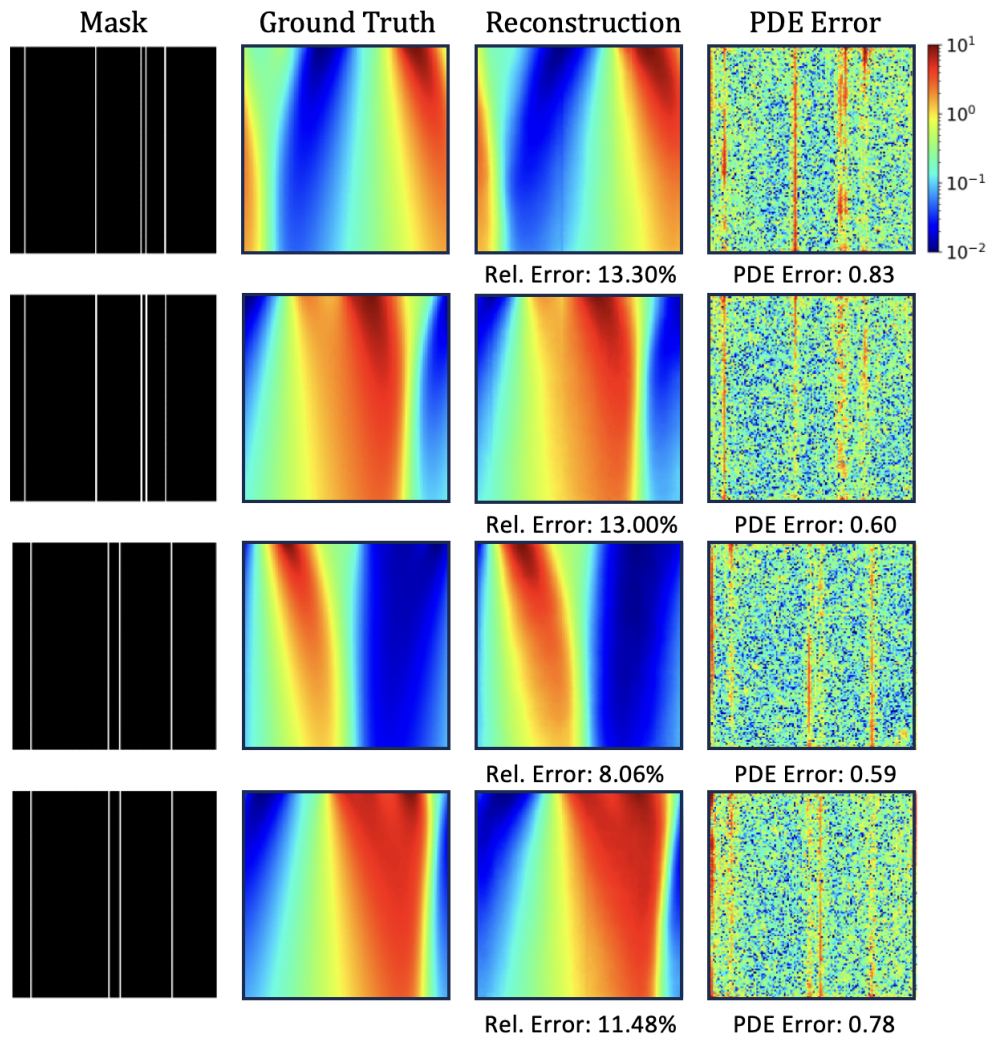


Figure 8 | Qualitative result for the reconstruction problem of Burgers' equation. The mask column shows where the 5 sensors are placed (3.9% partial observation). The PDE error column shows the pointwise absolute error $|r(\mathbf{x})_i|$ over the grid (log-scaled colorbar).